AD-A137 167 JOINT AGENCY TURBULENCE EXPERIMENT(U) AIR FORCE GEOPHYSICS LAB HANSCOM AFB MA A R BOHNE 13 JUL 83 AFGL-TR-83-0180 1/1

UNCLASSIFIED F/G 4/2 NL

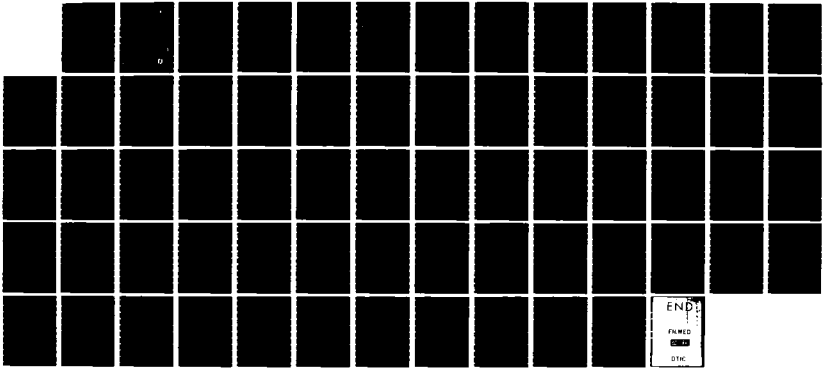

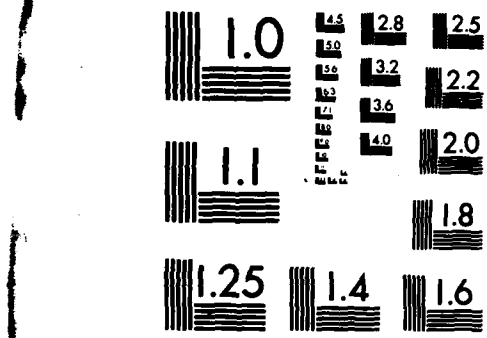

(12)

AFGL-TR-83-0180
ENVIRONMENTAL RESEARCH PAPERS, NO. 844

Joint Agency Turbulence Experiment Interim Report

ALAN R. BOHNE

13 July 1983

METEOROLOGY DIVISION PROJECT 6670
AIR FORCE GEOPHYSICS LABORATORY
HANSCOM AFB, MASSACHUSETTS 01731

AIR FORCE SYSTEMS COMMAND, USAF

This report has been reviewed by the ESD Public Affairs Office (PA) and is releasable to the National Technical Information Service (NTIS).

This technical report has been reviewed and is approved for publication.

FOR THE COMMANDER

KENNETH M. GLOVER
Chief, Ground Based Remote Sensing Branch
Meteorology Division

ROBERT A. MCCLATCHEY
Director, Meteorology Division

Qualified requestors may obtain additional copies from the Defense Technical Information Center. All others should apply to the National Technical Information Service.

If your address has changed, or if you wish to be removed from the mailing list, or if the addressee is no longer employed by your organization, please notify AFGL/DAA, Hanscom AFB, MA 01731. This will assist us in maintaining a current mailing list.

Do not return copies of this report unless contractual obligations or notices on a specific document requires that it be returned.

Unclassified

SECURITY CLASSIFICATION OF THIS PAGE (When Data Entered)

REPORT DOCUMENTATION PAGE	READ INSTRUCTIONS BEFORE COMPLETING FORM
1. REPORT NUMBER: AFGL-TR-83-0180	2. GOVT ACCESSION NO.: AD-A137167
	3. RECIPIENT'S CATALOG NUMBER
4. TITLE (and Subtitle): JOINT AGENCY TURBULENCE EXPERIMENT INTERIM REPORT	5. TYPE OF REPORT & PERIOD COVERED: Scientific. Interim.
	6. PERFORMING ORG. REPORT NUMBER: ERP No. 844
7. AUTHOR(s): Alan R. Bohne	8. CONTRACT OR GRANT NUMBER(s)
9. PERFORMING ORGANIZATION NAME AND ADDRESS: Air Force Geophysics Laboratory (LYR), Hanscom AFB, Massachusetts 01731	10. PROGRAM ELEMENT, PROJECT, TASK AREA & WORK UNIT NUMBERS: 62101F, 66701502
11. CONTROLLING OFFICE NAME AND ADDRESS: Air Force Geophysics Laboratory (LYR), Hanscom AFB, Massachusetts 01731	12. REPORT DATE: 13 July 1983
	13. NUMBER OF PAGES: 65
14. MONITORING AGENCY NAME & ADDRESS (if different from Controlling Office)	15. SECURITY CLASS. (of this report): Unclassified
	15a. DECLASSIFICATION DOWNGRADING SCHEDULE

16. DISTRIBUTION STATEMENT (of this Report)

Approved for public release; distribution unlimited.

17. DISTRIBUTION STATEMENT (of the abstract entered in Block 20, if different from Report)

18. SUPPLEMENTARY NOTES

19. KEY WORDS (Continue on reverse side if necessary and identify by block number)

Radar	Turbulence outer scale
Doppler radar	Eddy dissipation rate
Doppler spectrum mean	Structure function
Doppler spectrum variance	Turbulence severity
Turbulence	

20. ABSTRACT (Continue on reverse side if necessary and identify by block number)

Doppler radar data acquired during the 1981 Joint Agency Turbulence Experiment are presented. Pulse-pair processed reflectivity factor and Doppler spectrum mean data collected during volume scan periods are displayed over constant height surfaces at aircraft penetration level. Time histories of tracking-gate Doppler spectrum mean and variance data collected during aircraft storm penetration periods are also presented. These data show the Doppler spectrum variance to be poorly correlated with gradients of the radial wind, suggesting turbulence is the dominant contributor

DD FORM 1 JAN 73 1473 EDITION OF 1 NOV 65 IS OBSOLETE

Unclassified

SECURITY CLASSIFICATION OF THIS PAGE (When Data Entered)

20. Abstract (Contd)

to Doppler spectrum variance. The data show that areas of moderate to heavy turbulence are distributed throughout the storms. Estimations of turbulence severity are obtained through structure function and Doppler spectrum variance methods. Qualitative results suggest that for observations taken at moderate to long range, storm structure wind shear can strongly bias structure function estimates of turbulence severity, but generally have little influence on estimates from variance methods. The effective turbulence outer scale, the maximum eddy size when the turbulence field is represented by the Kolmogorov inertial subrange law, is typically less than 2 km.

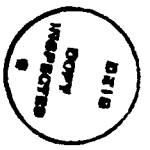

Preface

The successful operation of the Joint Agency Turbulence Experiment was the result of a huge effort expended by a large number of dedicated researchers. Coordination of the NASA Langley Research Center F106B aircraft and the NASA Wallops Flight Center SPANDAR radar required a great degree of communication and coordination between the personnel of these two agencies and AFGL. Particular thanks are given to Norman Crabill, Program Manager of the NASA Langley Storm Hazards Program, and Bruce Fisher, Project Engineer. At NASA Wallops, Robert Carr, Project Manager and Instrumentation Coordinator, Jack Howard and George Bishop, Chiefs of the SPANDAR group, Norman Beasley and the rest of the group were also invaluable. A large contingent of AFGL staff, including Ken Glover, Chief of the Ground Based Remote Sensing Branch, Ken Banis, Alexander Bishop, Maj. Carl Bjerkaas, Don Fitzgerald, and Pio Petrocchi provided valuable input and/or shared the responsibility of maintaining or directing the AFGL effort at Wallops Island. Particular thanks are directed to Graham Armstrong for designing the AFGL tracking system in addition to participating in taking observations at Wallops Island. I am sincerely indebted to Bill Smith and Maj. Doug Forsyth for their extensive participation and important roles in maintaining and directing the AFGL effort at Wallops Island. I also wish to thank Albert Chmela for his assistance in data reduction.

Contents

Illustrations

Joint Agency Turbulence Experiment Interim Report

1. INTRODUCTION

The Air Force Geophysics Laboratory (AFGL) is developing an airborne remote turbulence sensor to enable pilots to avoid regions of turbulence that are hazardous to aircraft. Methodologies developed at AFGL were initially tested with ground-based radar and aircraft gust data acquired from the 1976 Rough Rider program. During this experiment, the National Severe Storms Laboratory Norman Doppler radar performed periodic sector scans of a storm while an Air Force F4 Phantom aircraft, equipped with lightning and vertical gust measurement equipment, made storm penetrations. During these penetrations aircraft measurements were made from which the vertical gust velocities were derived.

These radar and aircraft data were previously analyzed and reported (Bohne[1, 2]). The results of these observations showed definite promise in the use of radar to detect and quantify regions of turbulence in storms.

(Received for publication 1 July 1983)

1. Bohne, A.R. (1981a) Radar Detection of Turbulence in Thunderstorms, AFGL-TR-81-0102, AD A108679.

2. Bohne, A.R. (1981b) Estimation of turbulence severity in precipitation environments by radar, Preprints, 20th Radar Meteorology Conference, Amer. Meteor. Soc., Boston, Mass., pp. 446-453.

To increase the data base and resolve some of the discrepancies observed in this early data, a more coordinated set of data was required. To this aim AFGL established the Joint Agency Turbulence Experiment and participated in the Storm Hazards Program at Wallops Island, Virginia, with NASA Langley Research Center and the NASA Wallops Flight Center during the early summer months of 1981 and 1982. This effort utilized ground-based and tracking radars, a lightning and gust measurement equipped F106B aircraft, and other ground-based sensors to study the effects of lightning and turbulence on aircraft.

The particular aim of AFGL was to obtain ground-based radar and in-situ aircraft gust data that were spatially and temporally coincident. The AFGL incorporated Doppler processing and recording equipment into the Wallops Island SPANDAR radar system. This radar, with a 0.41° full half-power beam width and wavelength of 10.56 cm, was operated at 320, 640, or 1280 prf, which thus afforded unambiguous ranges and velocities of 468, 234, and 117 km and 33.79, 16.90, and 8.45 m/s, respectively.

The time and space coincident aircraft and radar data acquired during these tests are being used to further test the AFGL turbulence detection methodology, and to provide useful information on the state of the turbulent atmosphere. The data presented here are observations of the data structure and environments from the 1981 season. The integrated radar-aircraft analysis results will appear in a later report.

2. OPERATIONAL MODE

Two different radar data sets, tracking and general coverage, were recorded by AFGL. During aircraft storm penetrations, the aircraft was tracked by the SPANDAR radar. This was accomplished by slaving SPANDAR, parallax corrected, to a nearby tracking radar. Using the aircraft position information supplied by the tracking radar, six contiguous tracking gates were locked onto the aircraft position. The aircraft was kept in a selected tracking gate to ensure that the aircraft track was being maintained. The tracking gate data recorded were the pulse-to-pulse in-phase and quadrature Doppler returns and ancillary information. Real-time monitoring was accomplished by sampling tracking gate data with a Ubiquitous Spectrum Analyzer and observing the aircraft spike in the one-dimensional Doppler spectrum. The data were recorded in analog mode on an Ampex FR1300 recorder.

Between storm penetrations, AFGL collected Doppler radar data in sector scan mode. Typically 768 or 1024 1-μsec gates, contiguous or with a 1-μsec spacing, were scanned over a 30° to 60° sector with three to five elevation steps.

The reflectivity factor and Doppler spectrum mean and variance were developed in real time by the hardwired pulse-pair processor and recorded on the AFGL archiving system. The sector scan data were used to provide real-time aircraft hazard avoidance information to aid in selecting the penetration routes for the F106B, and to provide general storm surveillance.

During storm penetrations the F106B equipment, in addition to making extensive lightning strike, atmospheric chemical, and multi-wavelength observations, made gust parameter measurements of the three components of wind gust velocity. These measurements, made at the rate of 80/s, were later sampled and digitized at the rate of 20/s. The measurements were then used to derive the longitudin transverse, and vertical gust velocity estimates. These data will provide the 'ground truth' measurements against which the radar data will be compared, a will provide further information on the state of the atmosphere, which is diffic to assess from the radar data alone.

3. DATA REDUCTION

The tracking gate data consisted of pulse-to-pulse measurements of the in-phase and quadrature sampled return and associated housekeeping. These tracking data were recorded in analog fashion on fourteen track tape. All data were initially reviewed with use of a Ubiquitous Spectrum Analyzer to identify those gates in which aircraft contamination was present. One of the gates from each penetration was then digitized for use in later analyses. Typically, the uncontaminated gate between the radar and the aircraft closest to the plane was used. It was observed that, with the aircraft located near the middle of the six contiguous tracking gates, the first and last pair of gates (1, 2 and 5, 6) were not contaminated. The selected data were then digitized and recorded as 256 (128 real and imaginary) sample records. For comparison purposes, three different estimators were employed to determine Doppler spectrum mean and variance. These included pulse pair, objective thresholding, and constant threshold from the spectrum peak. The algorithms employ standard autocorrelation and FFT techniques and include automatic image spectrum removal and velocity unfolding.

Because the aircraft was frequently in precipitation sparse regions, small segments of missing data were occasionally observed in the time histories of the track data. Analyses of the radar radial velocity data include autocorrelation, structure function, and power spectrum analysis methods. To implement these most easily it is necessary to have continuous time histories of data. To remove the gaps (one to six missing consecutive data values) the mean value and variance of the parameter in question was estimated for a small neighborhood of values on

each side of the data gap. The mean values established a linear trend across the data gap. The trend values were then modified by adding a random value at each missing data location. The family of random values used had a variance that was similar to that observed in the neighboring areas. The fitted regions were found visually undetectable against the background of true neighboring data. Although this technique does not replicate the true missing data, the fitted segments are so small in number and extent in contrast to the original total time histories that little distortion of energy content at the frequencies of concern are expected.

Further editing was occasionally required to remove spurious spectral estimates believed to result from occasional wavering of the tracking gate location about the aircraft position. The AFGL system used the tracking information supplied to the SPANDAR radar to update the tracking gates at a rate of 10 s. This time interval represents an aircraft movement of roughly 10 m between updates. This is small, however, in comparison to the AFGL tracking range resolution of 60 m.

Of added concern are the effects of the occasional large ranges of the storms penetrated. Here, small pointing errors could easily move the tracking gates by a few hundreds of meters. The combination of the range stepping update of the AFGL system with a slight pointing error could result in the time series data being used to derive a single Doppler spectrum to be obtained from nearly separate spatial locations, possibly exhibiting different wind characteristics. This is believed to be primarily responsible for the spurious results observed. The above-mentioned procedures were performed on both the Doppler spectrum velocity and variance data.

4. DATA PRESENTATION

4.1 Sounding Data

The environmental soundings to be shown represent estimates of the structure at the time and location of observations. Generally, the observation periods occurred in between standard sounding locations and times. To obtain a representative sounding, the Wallops Island and other nearest sounding station data from the earlier and later sounding periods were used to construct a best-fit sounding for the time and location desired. Due to the close proximity of the storms to Wallops Island, however, these best-fit soundings were nearly identical to the Wallops Island soundings alone. Thus, the use of interpolated soundings was abandoned and only Wallops Island data are used here. Although the accuracy of the temperature data are of some concern, the environmental wind structure, as observed from the storm radial velocity data, agrees well with the Wallops Island sounding wind structure.

4.2 Cartesian Representation of Sector Scan Data

The data acquired during the sector scan portion of storm observations are interpolated to a Cartesian grid system. The data are the equivalent reflectivity factor and the Doppler mean velocity at storm penetration altitude. This level was determined from the radar computed tracking altitude, rather than from the aircraft determined altitude, to ensure proper accounting for Earth curvature and index of refraction effects. The reflectivity factor and radial velocity structures were observed over a few sector scans where possible to determine an advection velocity for each storm during the observation period. This advection velocity was then applied to all scan data to ensure that the data were interpolated to the proper grid-point locations. In all cases this advection velocity is in good agreement with the estimated sounding velocity for the observational period.

Often a number of aircraft storm penetrations were performed before a complete sector scan update could be obtained. In this instance, a single representative Cartesian data set, with the aircraft penetration tracks advected to the proper storm locations as determined by the storm advection velocity, is used. Now, however, comparisons between aircraft and radar scan data do require a relatively stationary storm structure. Those cases where significant evolution was observed between the time of aircraft storm penetrations and the sector scan period are noted. The grid-point separations in these plots range from 0.5 to 1.5 km in the horizontal and 0.5 to 1.0 km in the vertical. The occasional coarse resolution is a result of the limited number of sector scans performed between penetrations and the large range of the storms from the SPANDAR radar. Finally, since a 15-dBZ threshold is used in the plotting of the reflectivity data, the plots do not represent the entire spatial extent of the storms.

4.3 Tracking Data

The tracking gate Doppler data displayed are the Doppler spectrum mean velocity and variance. The data presented are a smoothed version of the original data and were obtained by applying a simple constant nine-point filter on the nine nearest neighbor values centered about the data point in question. The smoothed data show more clearly the trend in the data and allow easier comparison of radar spectrum data with storm structure encountered along the aircraft track. This filter will not be employed in future power spectrum analysis.

4.4 Turbulence Severity Estimates

The parameter of interest here is the eddy dissipation rate (ϵ), which represents the rate of transfer of turbulence kinetic energy from larger to smaller

scales of motion, or eddies. The turbulence severity index, simply the cube root of ϵ, has been offered (MacCready[3]) as a means of quantifying the degree of hazard to aircraft penetrating a given region of turbulence. Radar estimates of eddy dissipation rate (ϵ) along the aircraft penetration tracks are determined using two different methods. First, the tracking gate Doppler velocity data are used in a structure function analysis, which essentially measures the degree of correlation of radar radial velocity data with distance. Second, the tracking gate Doppler spectrum variance (DSV) data are related to the eddy dissipation rate via a relation founded on the concept that the turbulent air and precipitation motions, particularly at scales primarily less than the maximum pulse volume dimension, are mapped into DSV. The relation used is that derived by Frisch and Clifford,[4] which assumes a turbulence outer scale (effective maximum eddy size in the inertial subrange) of infinity. The more accurate method which employs use of actual estimates of the turbulence outer scale to relate spectrum variance and ϵ were not made at this time. The following material briefly outlines the manner in which the two methods were employed.

The form of the one-dimensional structure function used is

$$D(r) = (D_l(r) - D_t(r))(x_l/r)^2 + D_t(r) \quad (1)$$

$$= \langle (V(R) - V(R + r))^2 \rangle \quad , \quad (2)$$

where $D_l(r)$ and $D_t(r)$ are the one-dimensional longitudinal and transverse structure functions, respectively, and are given by

$$D_l(r) = C(\epsilon\, r)^{(2/3)} \quad (3)$$

$$D_t(r) = 4/3\ C(\epsilon\, r)^{(2/3)} \quad , \quad (4)$$

for the inertial subrange region of a homogeneous isotropic turbulence field. This relation is required since the aircraft penetration tracks were neither parallel nor orthogonal to the radar viewing direction. In these relations C is a universal constant (1.77), r is the distance interval between successive radar velocity measurements used to form the estimate, and X_l is the component of this distance along the radar viewing direction.

---

3. MacCready, P. (1964) Standardization of gustiness values from aircraft, J. Appl. Meteorol. 13:808-811.

4. Frisch, A.S., and Clifford, S.P. (1974) A study of convection capped by a stable layer using Doppler radar and acoustic echo sounders, J. Atmos. Sci. 31:1622-1628.

As written, this relation portrays the behavior for an ensemble of structure functions derived from point velocity measurements in the turbulent field. However, when using radar radial velocity values, the random fluctuation in Doppler velocity arising from turbulence scales less than the maximum pulse volume dimension may be strongly filtered out. Thus, the radar structure function estimates, at least for the case of an ensemble of measurements, will be diminished in magnitude and contain proportionately greater amounts of energy from the larger scales of motion.

The mode of movement of the tracking gates alternated from one of nearly uniform scanning to a 1-μsec range jump as the plane moved in or out in range. Thus, the tracking gate data comprising the continuous time histories are not uniformly spaced. To obtain a more spatially uniform data set for use in the structure function analyses, only those data that were obtained immediately after a range jump are employed. This results in basic data sets where successive velocity values are 150 to 240 m apart. The structure function estimates at each data point location are derived from a local data set centered around the data point location of interest. These local data sets varied in length from 3 to 6 km.

The estimates of ϵ determined by this method will exhibit some error. First, the structure function estimates are derived from a limited number of observations that may only loosely approximate an ensemble of observations. Second, the magnitude of ϵ is diminished due to pulse volume filtering action. Third, the estimates are biased through incorporation of nonturbulent storm structure wind shear. Fourth, each velocity value naturally includes a random error component related to Doppler spectrum breadth and sample dwell time. This may add from 0.1 to 0.4 $(m/s)^2$ to the structure function magnitude.

In an attempt to account for these effects, the local data sets are first linearly detrended and eddy dissipation rate estimates are determined at the smallest length scales where the $r^{2/3}$ behavior is reasonably well observed, typically at length scales of 300 through 500 m.

The second method employed to estimate ϵ relies upon the relationship between DSV and the turbulent air motions. This method assumes some knowledge of the effective size of the largest turbulence eddies within the inertial subrange. The term effective is used since we are replacing the actual turbulence energy spectrum that contains energy-containing eddies, in addition to the inertial subrange, with a fully Kolmogorov energy spectrum form. If the actual Von Karman form of energy spectrum is known, or fine scale in-situ measurements are available, then the effective outer scale length may be determined. These data are not presently available, however. Thus the solution of Frisch and Clifford,[4] whereby the inertial subrange is assumed to extend to eddies of infinite size, is employed. The relationship used is

$$\text{Var} = 1.354\ C\ (\epsilon\ a)^{(2/3)}\ (1 - z/15 - (z^2)/105 - \ldots) \tag{5}$$

where C is a universal constant of value near 1.35, and z and a are related to effective pulse volume width ($R\theta$) and length (L) by

$$z = 1 - (L/R\theta)^2 \tag{6}$$

$$a = R\theta/(8 \ln 4)^{(1/2)} \quad . \tag{7}$$

At the large ranges investigated, the series term remains essentially constant at 0.93, yielding the working relation

$$\text{Var} = .0225\ C\ (\epsilon\ R)^{(2/3)} \quad . \tag{8}$$

The variance data used in these analyses are the companion data to the Doppler velocity data used in the structure function analyses. The DSV values are derived from block averaging all variance data contained in five successive range jump segments. Effectively, this is simply averaging DSV over a spatial range comparable to that used in the structure function analyses. Eddy dissipation rate is then determined using these averaged variance values.

It is important to note that the structure function and spectrum variance techniques rely upon different effects of the turbulent air (precipitation) motions on the radar Doppler spectrum parameters. First, the structure function relies upon the turbulent air motions being mapped into fluctuation of the Doppler velocity, and then relates this fluctuation with intensity of the turbulence field. In the form used here [Eq. (1)], no accounting for the pulse volume filtering effects, that is, transference of some of this fluctuation energy into Doppler spectrum breadth is performed. The variance method, on the other hand, relies upon the spectrum broadening effects, and does account for loss of measurable turbulence energy to the fluctuating mean velocity. However, the relation used here does not assume a finite outer scale length. Past experience has shown that a length λ_o of 0.5 to 1.5 km is usually appropriate, indicating use of Eq. (5) will underestimate ϵ. If the outer scale length is considerably larger than twice the maximum pulse volume dimension, then Eq. (5) is quite good.

Neglecting for the moment the various beam filtering, storm structure wind shear, and other bias and random errors discussed earlier, comparison of the time history patterns and the relative magnitudes of the two separate estimates of ϵ may provide some useful qualitative information on the turbulence severity, turbulence outer scale length, and presence of strong storm wind shear.

For example, the maximum pulse volume dimension is typically 0.6 to 1.4 km. With an ensemble of measurements, about 90 percent of the turbulence energy is mapped into DSV for turbulence fields having effective outer scale lengths up to 2.8 km. This is certainly within the range of expected values. The structure function estimates employ velocity values that are spatial averages over the pulse volume (roughly 150 by 1 km), and which are separated in distance by 150 to 240 m. If the turbulence is homogeneous and isotropic, and the structure function estimates (reasonably well) approximate an ensemble of measurements, then we would expect most turbulence energy to be mapped into DSV, with little mapped into the fluctuation of the mean velocity. Thus, if the meteorological field is basically turbulent and the outer scale length less than twice the maximum pulse volume dimension, then we expect the time histories of the two estimates to be similar in form, but with the structure function (STF) derived estimates to be smaller in magnitude than the DSV values. If the magnitudes are small and equal, and the patterns are similar, then the effective outer scale may be small enough to allow the DSV underestimate to approach the STF value.

If the DSV estimate varies in magnitude while the STF estimate is constant, then a change in the turbulence outer scale is indicated. If the DSV estimate is relatively constant, while the STF estimate varies significantly, then presence of wind shear biasing the STF estimate is suggested. This results from the fact that a simple transverse wind shear contribution to ϵ is approximately eight times greater for the STF than the DSV estimate at these ranges.

Thus, with this set of qualitative guidelines, and remaining mindful of the caveats mentioned earlier, some useful information concerning the turbulence structure may be derived. Finally, one must note that turbulence severity ($\epsilon^{(1/3)}$) is displayed, and differences in the magnitudes of ϵ from the STF and DSV estimates are much greater than shown on these plots.

5. DISCUSSION OF DATA

5.1 1 July 1981

The first data set was obtained on 1 July 1981 (day 182). Figure 1 shows the estimated environmental sounding data. The wind direction varies slowly from about 170° near the surface, to 120° at 6 km. Over this height the speed also increases slowly from about 14 to 20 m/s. The temperature data is suspect since the sounding shows the environment becoming very dry at 3-km height, whereas the penetration level, as determined by the F106B, was 4.57 km.

Figure 2 shows the reflectivity factor for the storm at the penetration altitude of the F106B. The time period over which the sector scan data were collected extends from 18:16:00 to 18:17:26 GMT. The plot is time-advected to represent

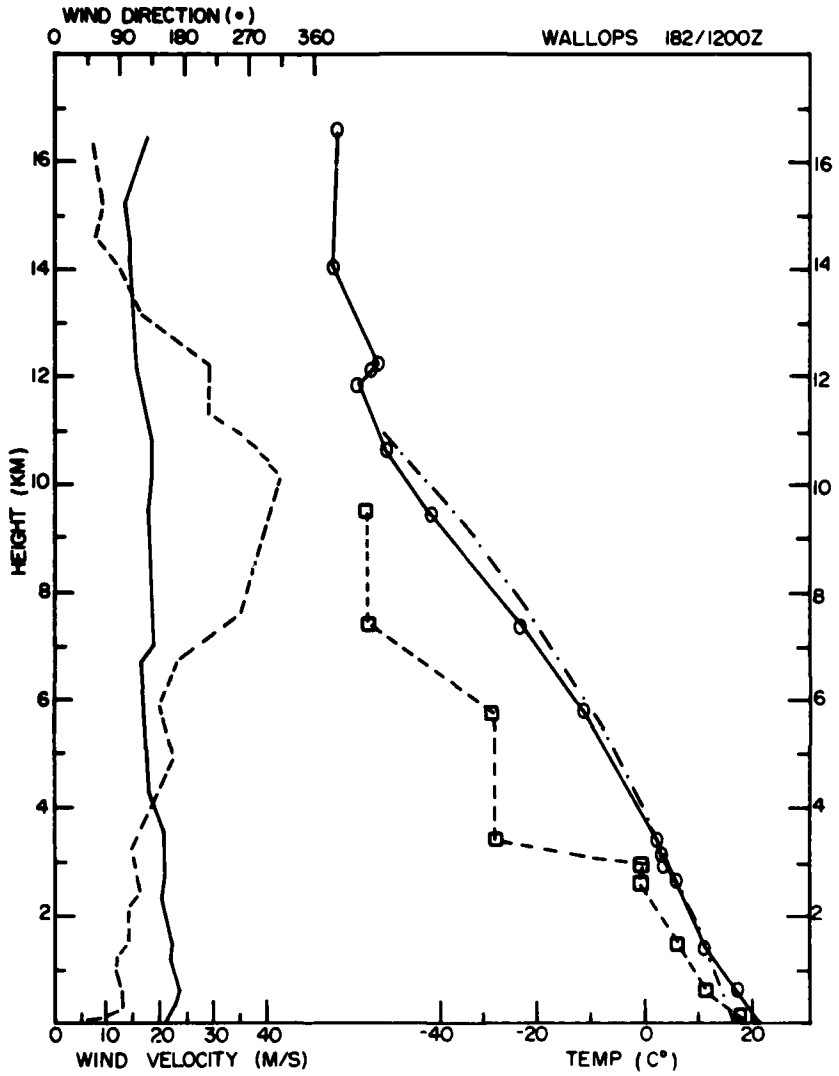

Figure 1. Wallops Island Sounding Data for 1 July 1981 at 1200 GMT. Wind data; speed (dash) and direction (solid): temperature; temperature (solid), dew point (dash), and pseudoadiabat (dash-dot)

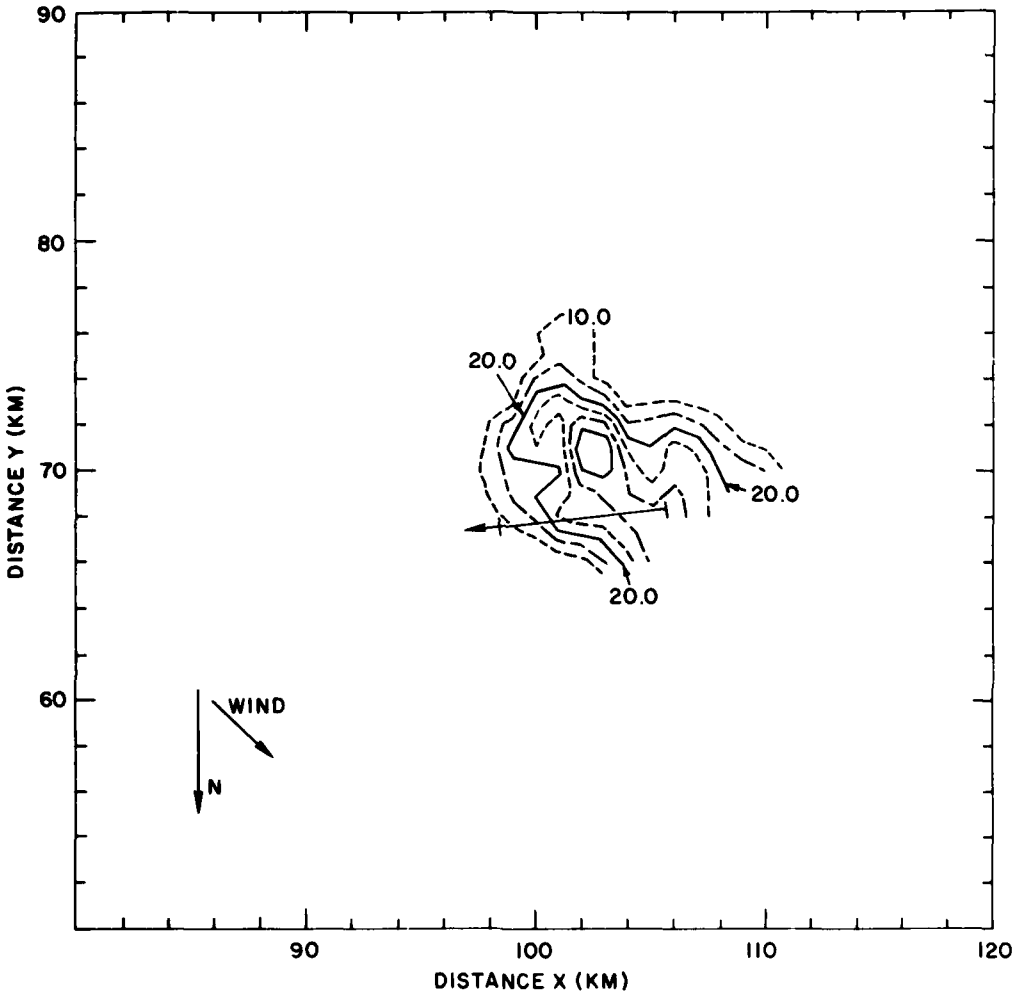

Figure 2. Contours of Storm Reflectivity Factor (dBZ) for 1 July 1981 on Constant Height Surface at Aircraft Storm Penetration Altitude of 4.57 km. Contours are in 5-dBZ increments with a recycling dot, dash, and solid pattern. Minimum contour value is 10 dBZ. Time-adjusted aircraft track is shown. Distances are relative to SPANDAR radar. Time is 18:17:00 GMT

the expected appearance at 18:17:00 GMT. The storm is seen to be small in extent (the northwest edge is not observed at this Cartesian grid level), roughly 200 km^2 in area. It is composed of a high reflectivity factor cell having maximum value near 40 dBZ. The storm is centered approximately 104 km west and 70 km south of the SPANDAR radar. Only one aircraft penetration was recorded this day. It covers the period from 18:17:00 to 18:17:55 GMT, and the time-adjusted track is shown in Figure 2. The observed track is about 11 km long and runs west to east. It begins near the center of the major storm cell at 106 km west and 68 km south of the radar, about 3 km north of the highest reflectivity factor cell, and extends to the radar storm boundary.

The sector scan radial velocity at this level is shown in Figure 3. The magnitude range is roughly -5 to +2 m/s. These small values are a result of the sector scan being oriented nearly orthogonally to the environmental wind. It is seen that the wind at the southwest portion of the storm is receding, while the northeast portion is moving towards the radar. The zero velocity line running southeast to northwest suggests some divergence in the environmental wind. This may indicate that the storm is blocking somewhat the onrushing environmental wind, causing it to turn northward on the northeast flank of the storm. The major cell penetrated exhibits a component towards the radar, which may be an indication of lower level air rising up into the storm.

The radar radial velocity time-history plot is shown in Figure 4. The observed velocities, with the small positive region near 18:17:38, agree well with variation along the track as depicted by the sector scan grid-point velocities. The corresponding tracking-gate spectral variance estimates, shown in Figure 5, vary from about 2 to 6 $(m/s)^2$. The variance peaks are well correlated with the regions of large gradient of the radial velocity (Figure 4). The somewhat periodic variations of magnitude in the velocity and variance plots exhibit periods in the range of 4 through 8 seconds. With an aircraft speed near 250 mi/hr, this translates into a length scale of 450 to 900 m, and may reflect some dominant perturbation scale regime initiated by the storm structure.

The turbulence severity estimates ($\epsilon^{1/3}$) are shown in Figure 6. The STF derived estimates show a steady increase from 1.5 $(cm^{2/3})/s$ at 18:17:25 GMT to a fairly constant value near 4 $(cm^{2/3})/s$ at 18:17:35 GMT and thereafter. The DSV derived estimates start near 5.5 $(cm^{2/3})/s$ and naturally vary in concert with the spectrum variance (Figure 5) values over a range of 3.5 to 4.5 $(cm^{2/3})/s$. With the DSV values being significantly greater than the STF estimates prior to 18:17:35 GMT, this region should exhibit relatively low shear, have most turbulence energy mapped into the DSV, and have an outer scale length less than twice the maximum pulse volume dimension. The period starting at 18:17:35 GMT shows quite good agreement in pattern and magnitude for the two estimates. The near

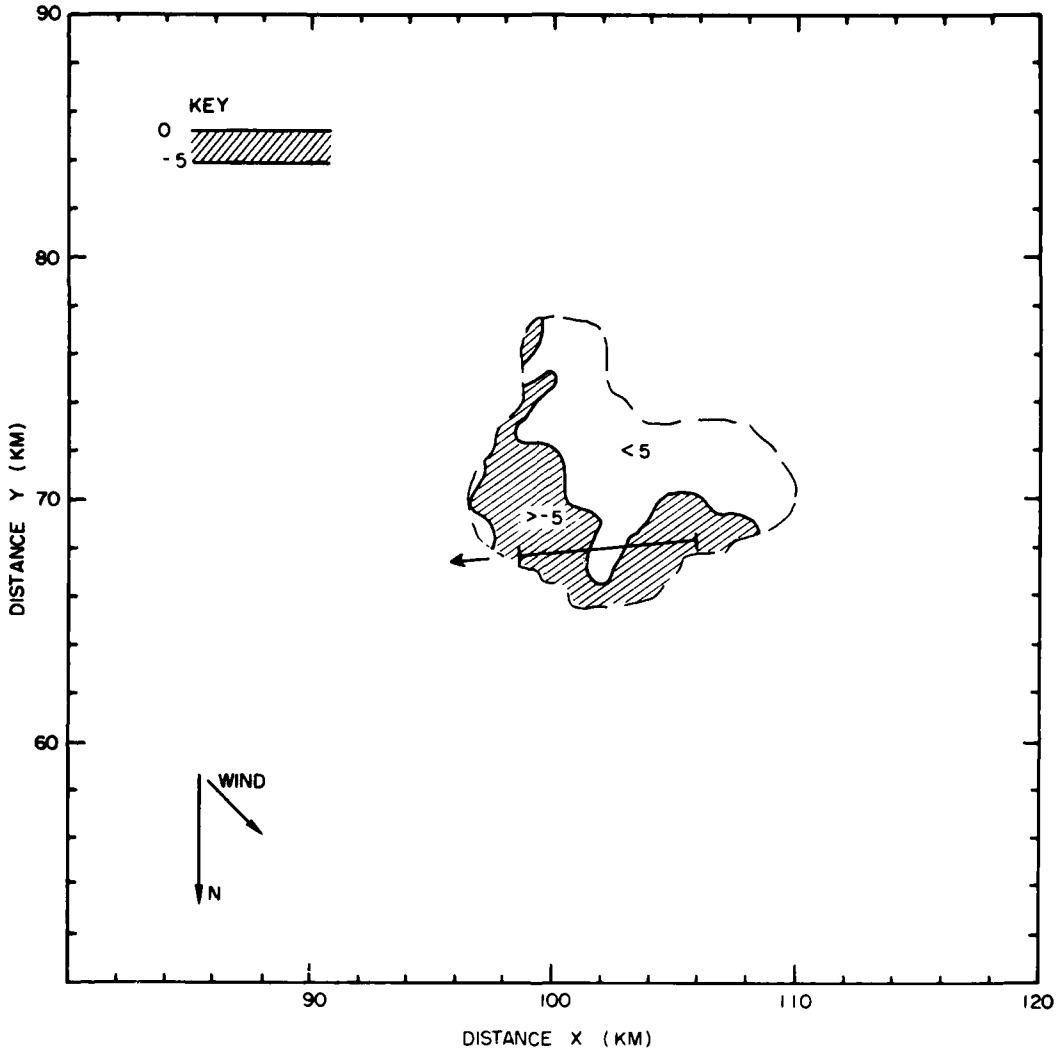

Figure 3. Contours of Doppler Radial Velocity in m/s for 1 July 1981 on Constant Height Surface at Aircraft Storm Penetration Altitude of 4.57 km. Contours are in 5-m/s increments. Time-adjusted aircraft track is shown. Distances are relative to SPANDAR radar. Positive values represent motion away from the radar. Time is 18:17:00 GMT

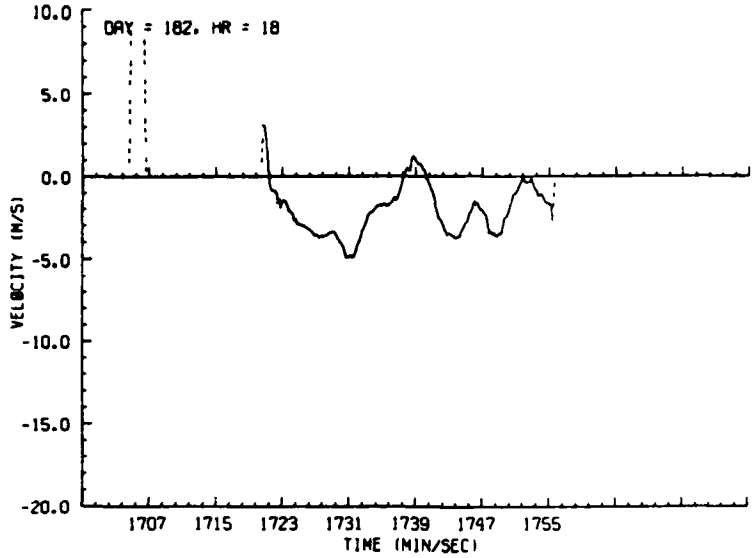

Figure 4. Time History Plot of Radar Radial Velocity for 1 July 1981 as Measured in Tracking Gate During Aircraft Storm Penetration. Dashed lines indicate missing data. A nine-point block filter has been applied to data

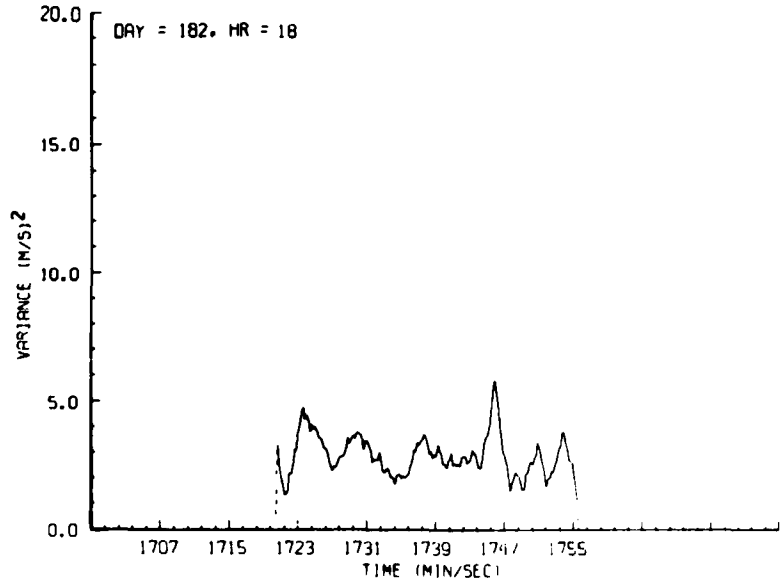

Figure 5. Time History Plot of Doppler Spectrum Variance (DSV) for 1 July 1981 as Measured in Tracking Gate During Storm Penetration. A nine-point block filter has been applied to data. Dash line represents missing data

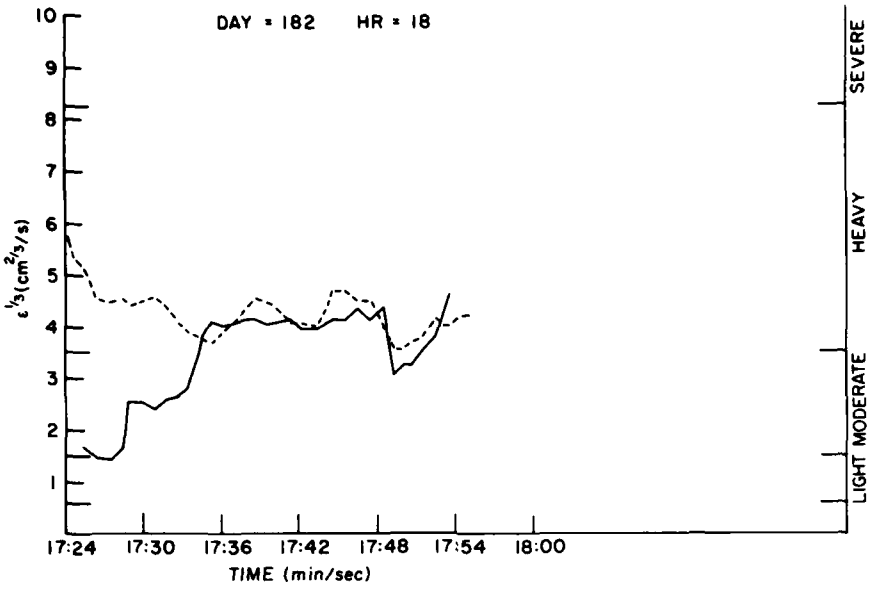

Figure 6. Time History Plot of Turbulence Severity ($\epsilon^{1/3}$) as Estimated by Doppler Spectrum Variance (DSV) (Dash) and Structure Function (Solid) Techniques for 1 July 1981

equality in value suggests an outer scale significantly less than the pulse volume width may be present. However, the DSV estimates remain roughly constant (except for a modulation), while the STF estimates increase to equal the DSV values. For this to be manifested by turbulence alone would necessitate ϵ to vary as $\lambda_0^{-5/3}$, an unlikely event. A more reasonable answer is that the fluctuation of the radial velocity (Figure 4) is more representative of storm wind structure effects. Then, the modulation of the DSV estimate during this period represents the contribution of this wind shear to the dominant turbulence component. Thus, the qualitative conclusion is that within the high reflectivity factor storm cell, little radial shear is present and most turbulence energy is mapped into the DSV. As the storm boundary is approached, the turbulence severity remains relatively constant, however, storm-structure wind shear increases. The effective outer scale length is less than 1.8 km throughout and the DSV appears to be clearly superior to the STF method used here.

5.2 3 July 1981

On 3 July 1981 (day 184) an extensive area of precipitation moved into the region from the southwest. The environmental sounding, Figure 7, shows both the wind direction and magnitude to be relatively constant at about 210° and 12 to

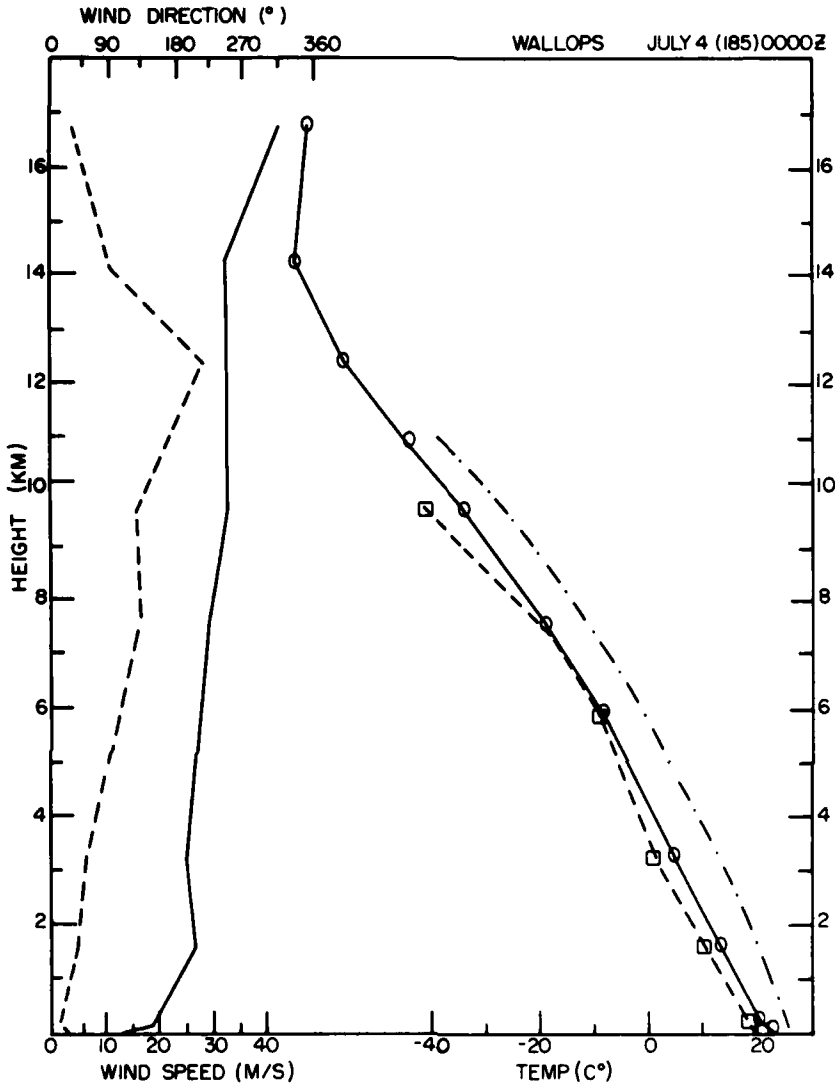

Figure 7. Sounding Data for 4 July 1981 at 00 GMT

15 m/s from 4 km to 9 km. Figure 8 displays the storm reflectivity factor at the penetration altitude of 4.87 km at 20:02:11 GMT. The region of interest consists of a central area of about 1800 km^2 and is located near 80 km west and 130 km the south of the SPANDAR radar. The area contains two high reflectivity factor cells with maximum values near 45 dBZ. The time-adjusted aircraft tracks are seen to extend across the effective storm width (20 to 20 dBZ contour), and pass partially through the two storm cells. The southwestern cell is in a state of decay. At the time of 20:15:32 GMT, this cell has essentially dissolved into the background with a maximum reflectivity factor of 25 dBz.

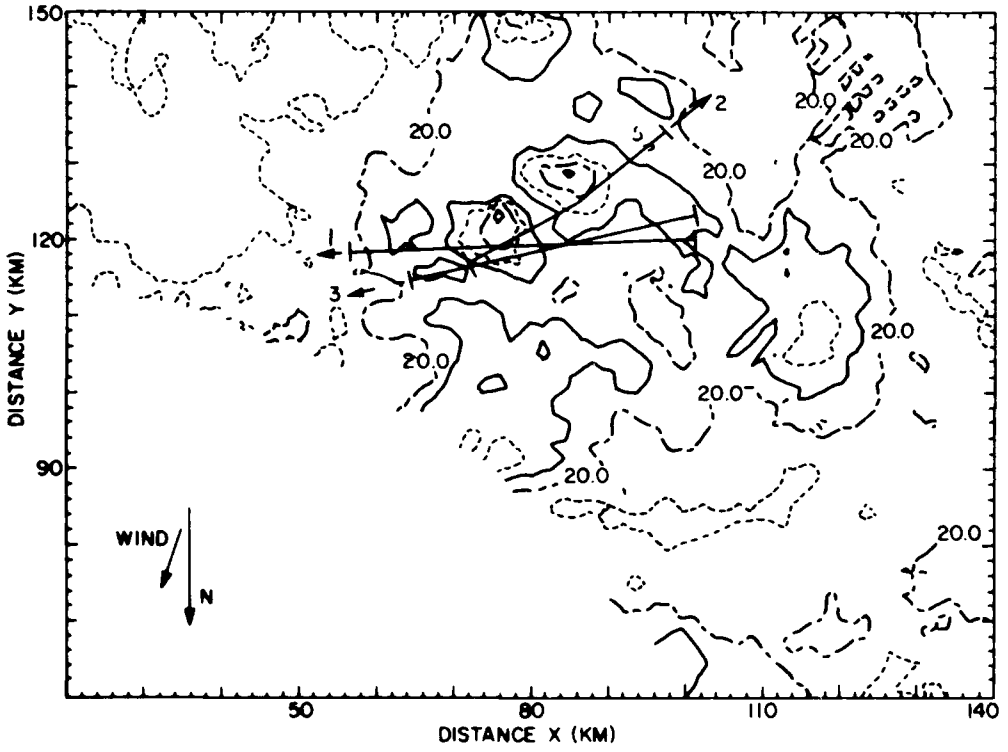

Fig. 8. Contours of Storm Reflectivity Factor at Penetration Altitude of 4.87 km for 3 July 1981 at 20:02:11 GMT. Minimum contour value is 15 dBZ.

The radial velocity values in Figure 9 range from about 0 to -20 m/s. Note that the radar is roughly looking along the wind near the area of storm penetration, with the aircraft tracks about 50 through 80° off the wind. The pattern of radial velocities show increased speed along the southeast and western boundary of the farther cell, with a minimum value on its upwind (southwest) side. The nearer cell also displays increased radial wind speed along its eastern boundary, but decreased speed along the western flank, just downwind of the further cell. Although the wind speed maximum along the eastern edge is primarily due to the radar pointing directly along the wind direction, these features suggest some blocking effects by the cells are occurring.

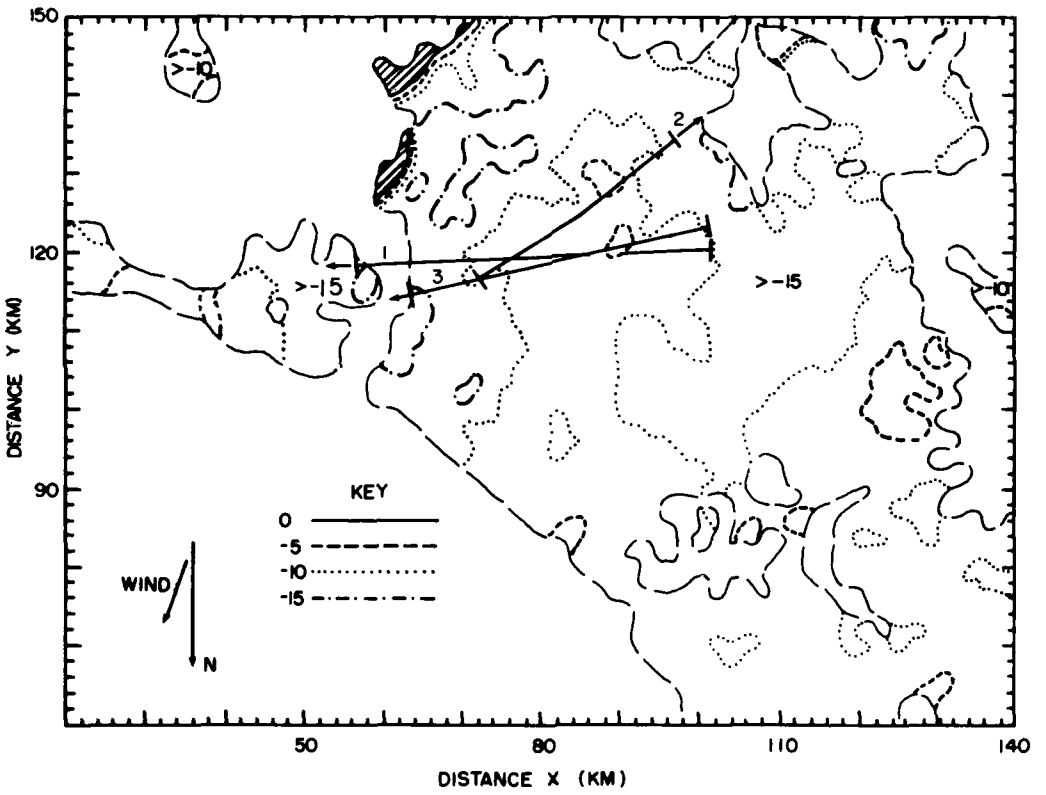

Figure 9. Contours of Storm Radial Velocity at Penetration Altitude of 4.87 km for 3 July 1981 at 20:02:11 GMT

The three tracking-gate radial velocity histories are shown in Figures 10 through 12. The magnitude ranges from about -18 to +1 m/s. These plots show in greater detail the significant modification of the environmental wind on the downwind side of the further cell (19:57:33 GMT), and the receding air motion within the cells themselves (20:04:45 GMT). These data agree well with the larger scale grid-point values of Figure 9.

The DSV plots, Figures 13 through 15, show the spectrum variance to be generally 0.5 to 2.0 $(m/s)^2$ away from the storm cells, but to have rapid and strong variation in the vicinity of the cells. For example, the large variation and peak magnitudes from 19:57:53 to 19:58:25 GMT of run 1 coincide with passage through the near storm cell. During the second penetration the two periods, 20:04:29 to 20:04:55 GMT and 20:05:36 to 20:05:50 GMT, generally coincide with passage through the two cells. The periods of large spectrum variance are most often not associated with any significant gradients of radial velocity. This suggests that pockets of strong turbulence rather than large-scale wind shear, are most often the cause for the large spectrum variances observed here. Last, the time histories exhibit fluctuations with periods in the ranges 3 to 8, 13 to 16, and 24 through 35 sec, or roughly 700, 1500, and 3500 m, respectively. The short period fluctuations appear as a ripple on the large period fluctuations. It is observed that the energy content increases dramatically with scale size.

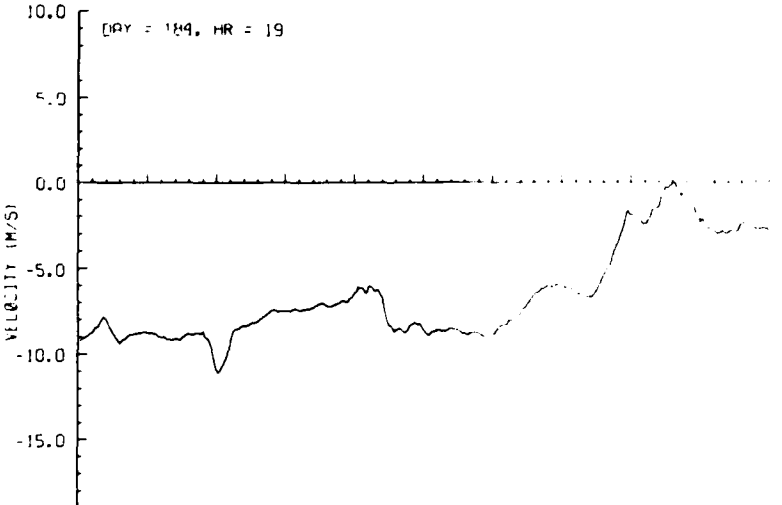

Figure 10. Time History Plot of Tracking Gate Radial Velocity for First Penetration at 4.87-km Altitude for 3 July 1981

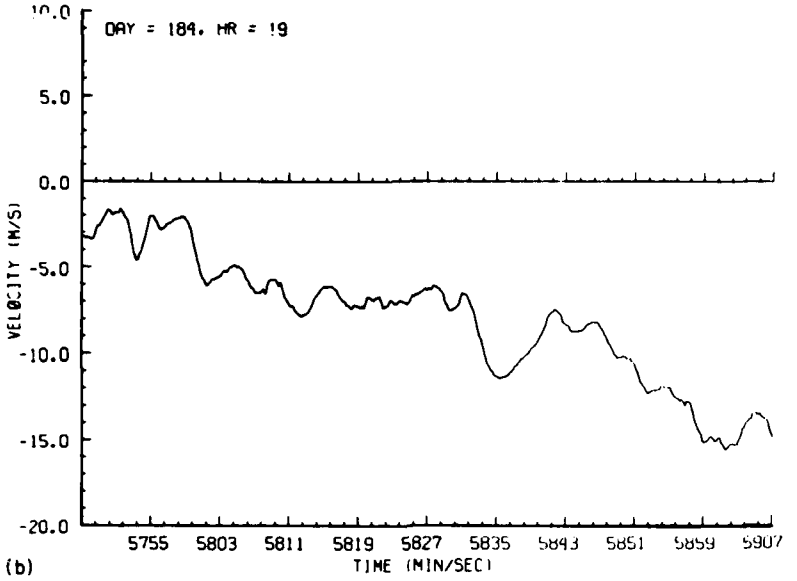

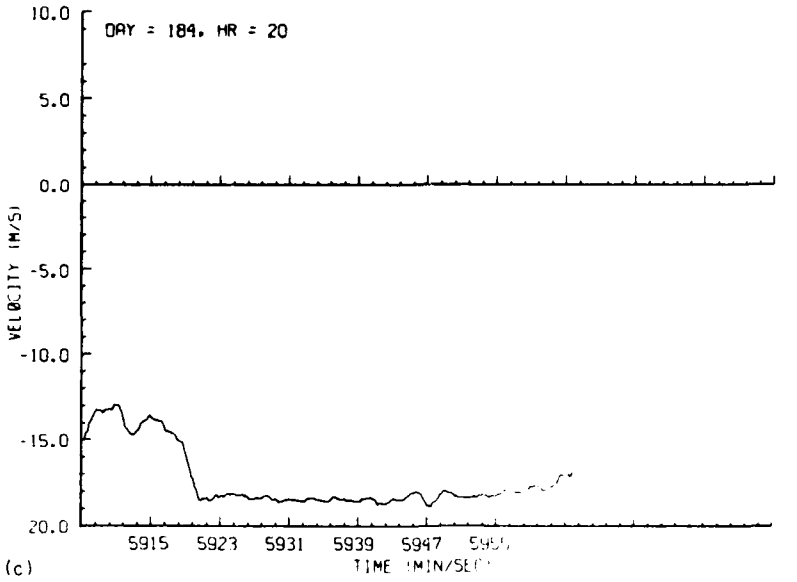

Figure 10. Time History Plot of Tracking Gate Radial Velocity for First Penetration at 4.87-km Altitude for 3 July 1981 (Contd)

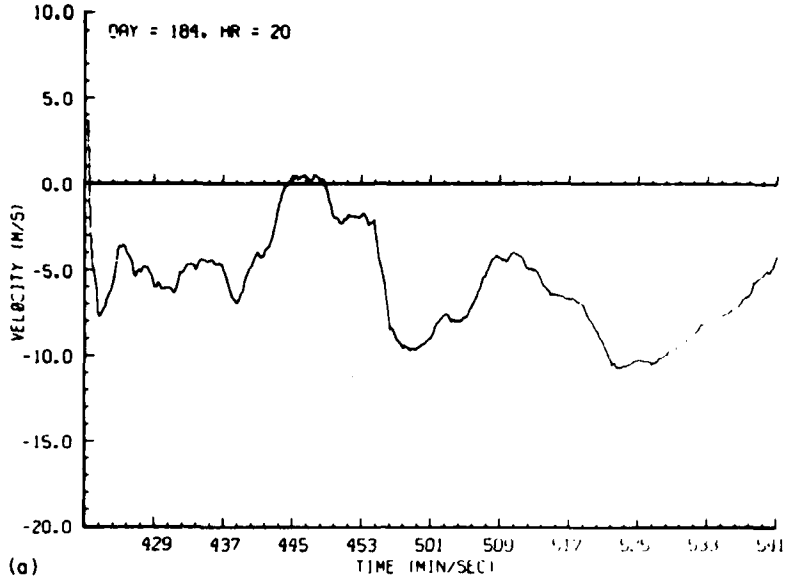

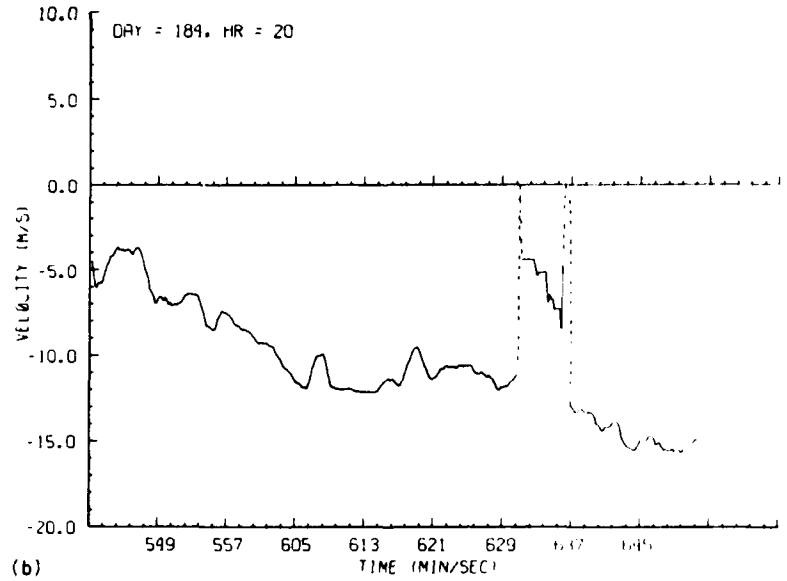

Figure 11. Time History Plot of Tracking Gate Radial Velocity for Second Recorded Penetration at 4.87-km Altitude for 3 July 1981

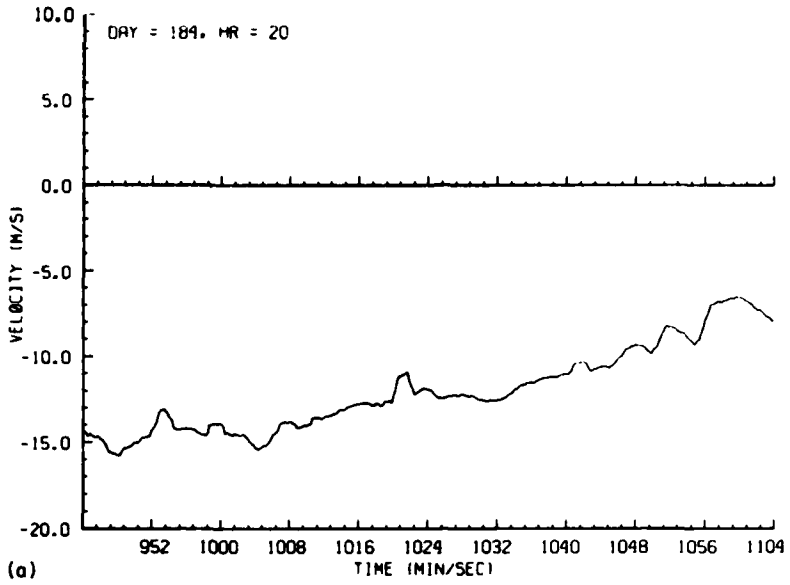

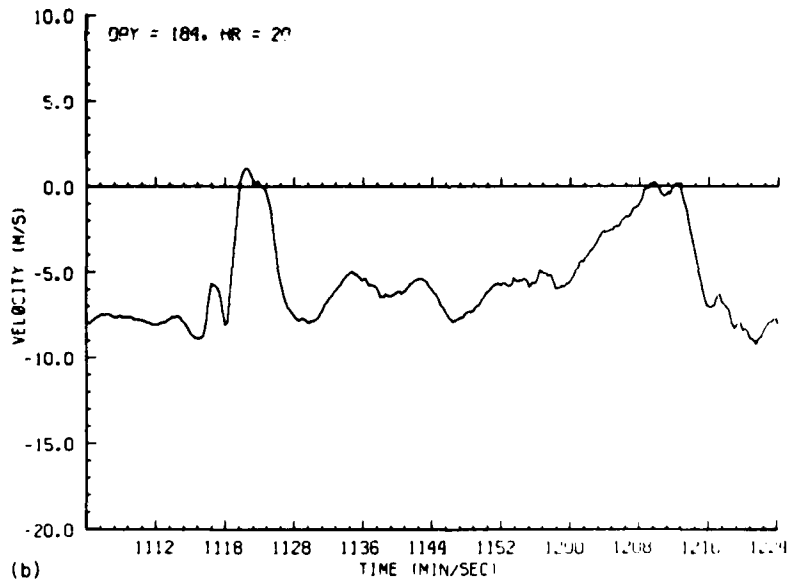

Figure 12. Time History Plot of Tracking Gate Radial Velocity for Third Recorded Penetration at 4.87-km Altitude on 3 July 1981

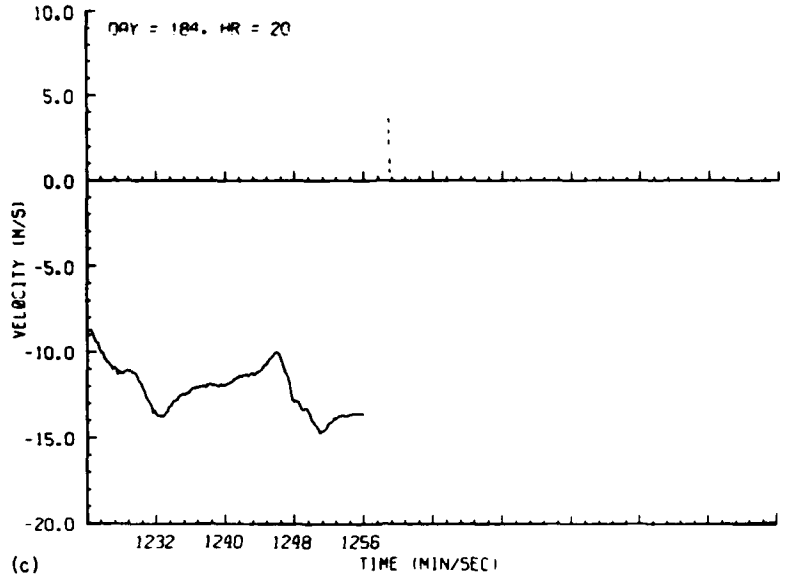

Figure 12. Time History Plot of Tracking Gate Radial Velocity for Third Recorded Penetration at 4.87-km Altitude on 3 July 1981 (Contd)

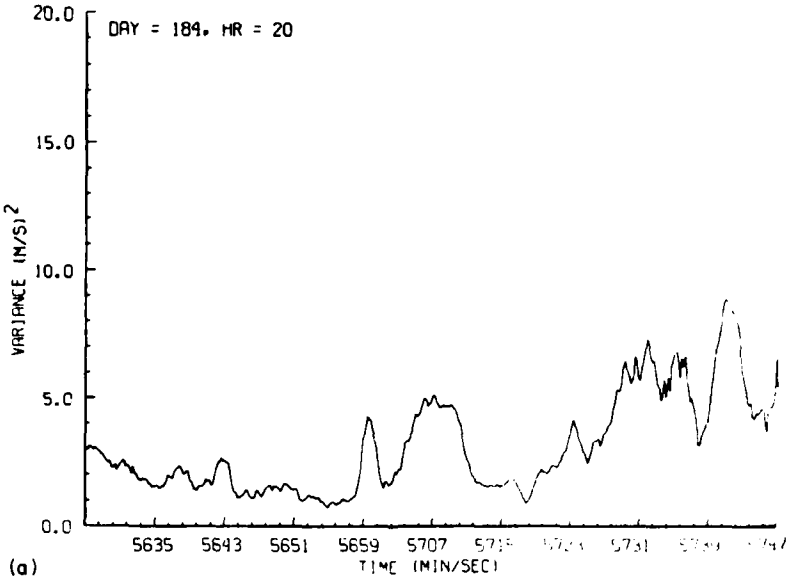

Figure 13. Time History Plot of Tracking Gate Doppler Spectrum Variance (DSV) for First Recorded Penetration at 4.87-km Altitude on 3 July 1981

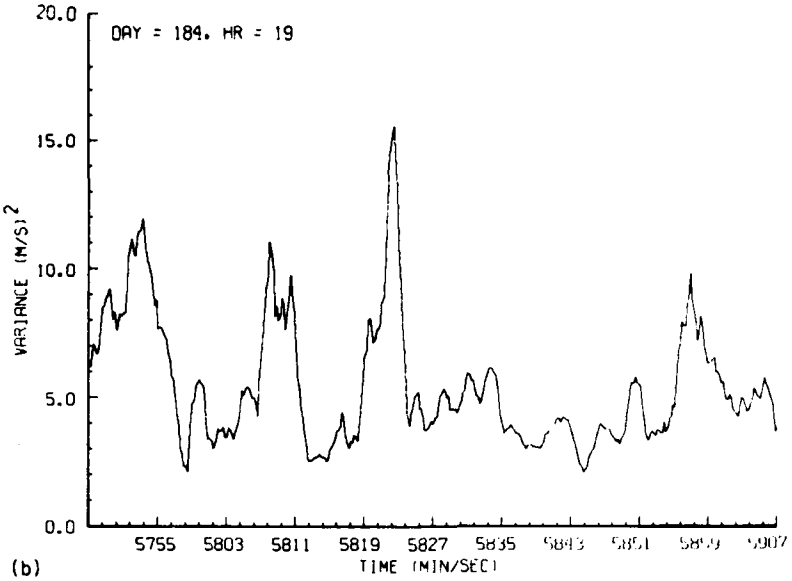

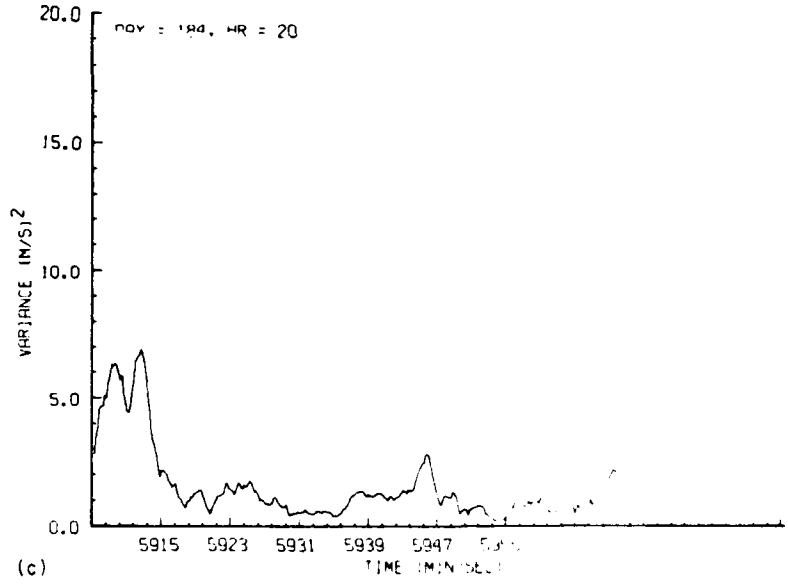

Figure 13. Time History Plot of Tracking Gate Doppler Spectrum Variance (DSV) for First Recorded Penetration at 4.87-km Altitude on 3 July 1981 (Contd)

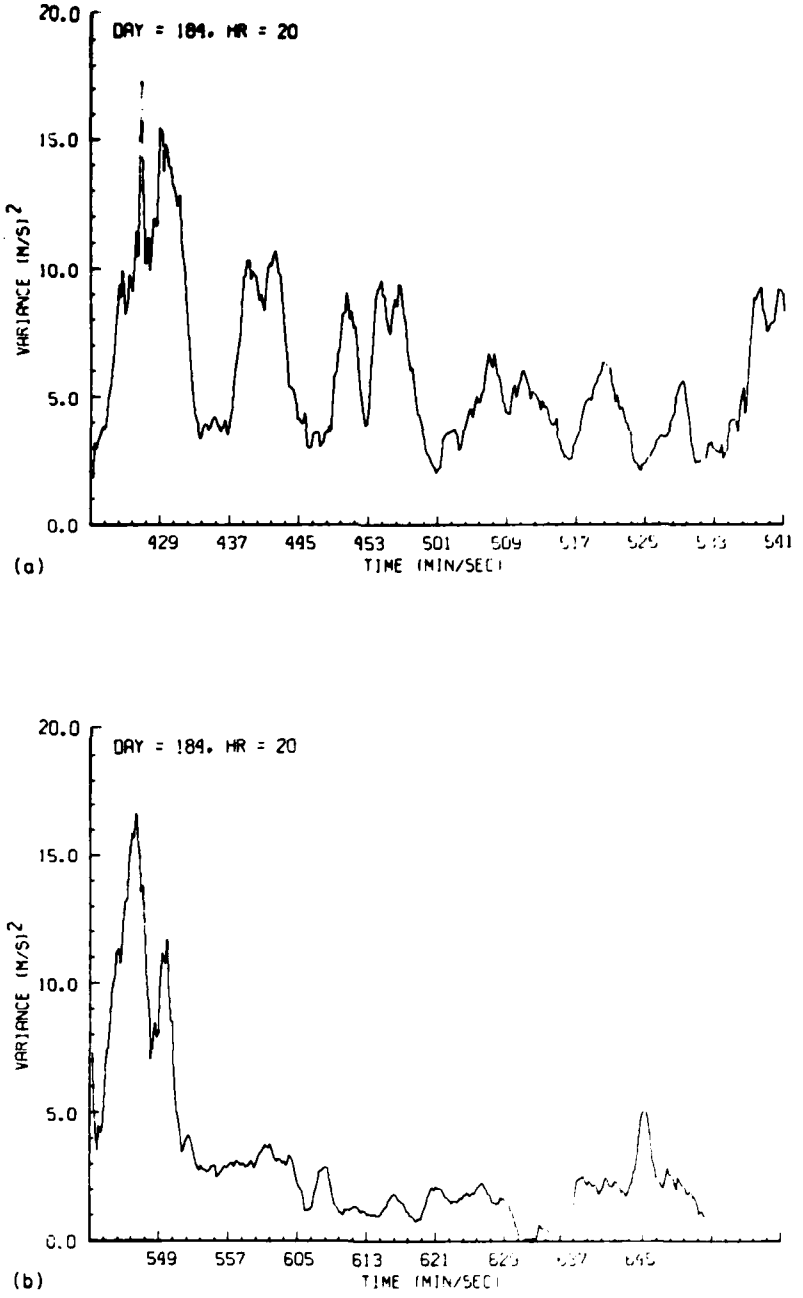

Figure 14. Time History Plot of Tracking Gate Doppler Spectrum Variance (DSV) for Second Recorded Penetration at 4.87-km Altitude on 3 July 1981

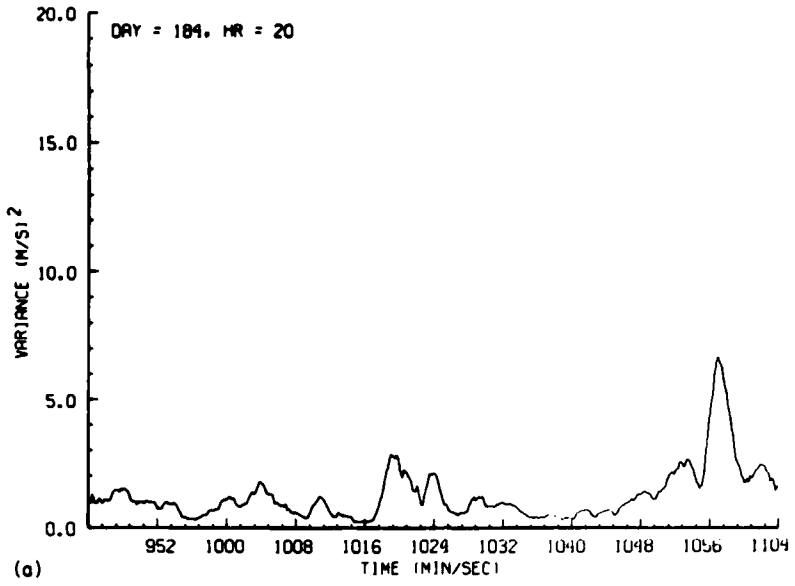

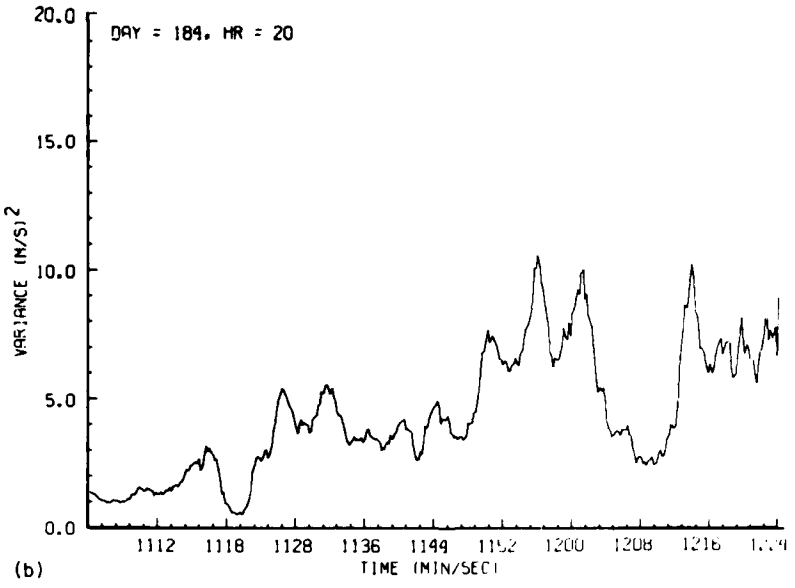

Figure 15. Time History Plot of Tracking Gate Doppler Spectrum Variance (DSV) for Third Recorded Penetration at 4.87-km Altitude on 3 July 1981

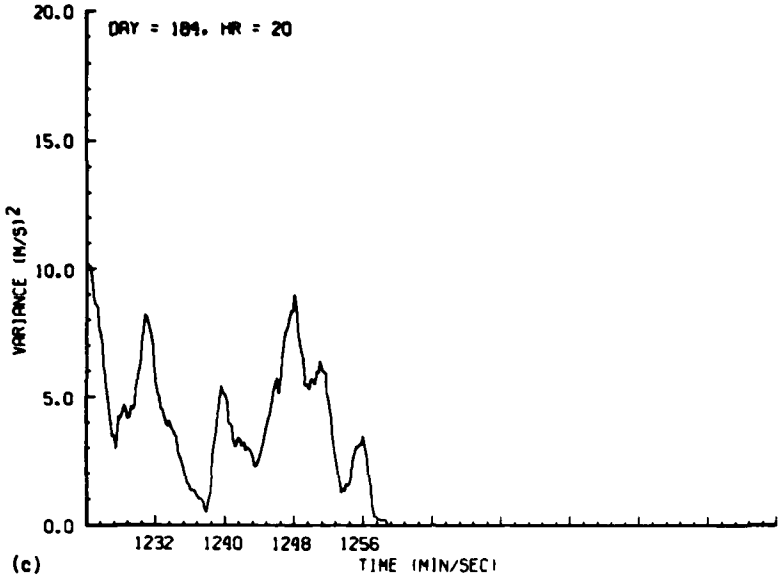

Figure 15. Time History Plot of Tracking Gate Doppler Spectrum Variance (DSV) for Third Recorded Penetration at 4.87-km Altitude on 3 July 1981 (Contd)

The turbulence severity estimates are displayed in Figures 16 through 18. The maximum pulse volume dimension is about 0.9 km. The first penetration track is about 55° off the viewing direction, thus the apparent shear of the radial velocity includes contributions from both longitudinal and transverse components of storm structure wind shear. The period up to 19:57:00 GMT shows the STF and DSV estimates to be small and nearly equal in magnitude. This region, exhibiting little radial shear and small DSV, suggests that turbulence is the main contributor to spectrum variance and the outer scale length is much smaller than twice the maximum pulse volume dimension, thus allowing for a large underestimate in the DSV value to approach the STF value. From 19:57:00 to 19:58:40 GMT the DSV estimates are considerably larger than the STF values and the two patterns are quite similar, suggesting turbulence is the prime contributor to spectrum variance and the outer scale has increased, but is still less than 1.8 km. The increasing severity from 19:57:00 to 19:58:00 GMT suggests relatively constant λ_o with increasing turbulence energy (ϵ) as the aircraft passes from downwind of the farther storm cell (88 km, 122 km) to the western boundary of the near cell (78 km, 120 km). The DSV turbulence severity within the near storm cell (19:58:00 to 19:59:00 GMT) is no greater than that found at the cell boundaries (25-dBZ contour) or on the downwind side of the farther cell (19:57:30 GMT).

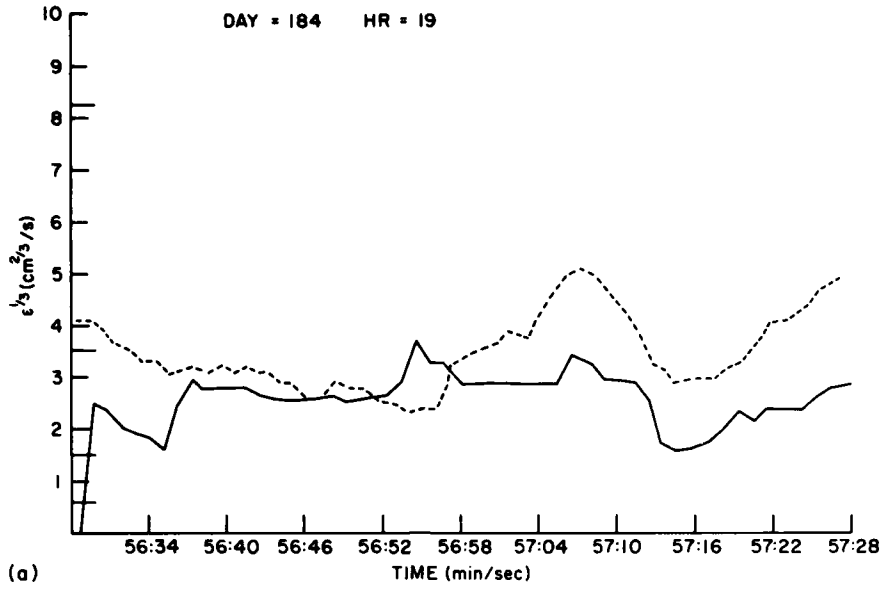

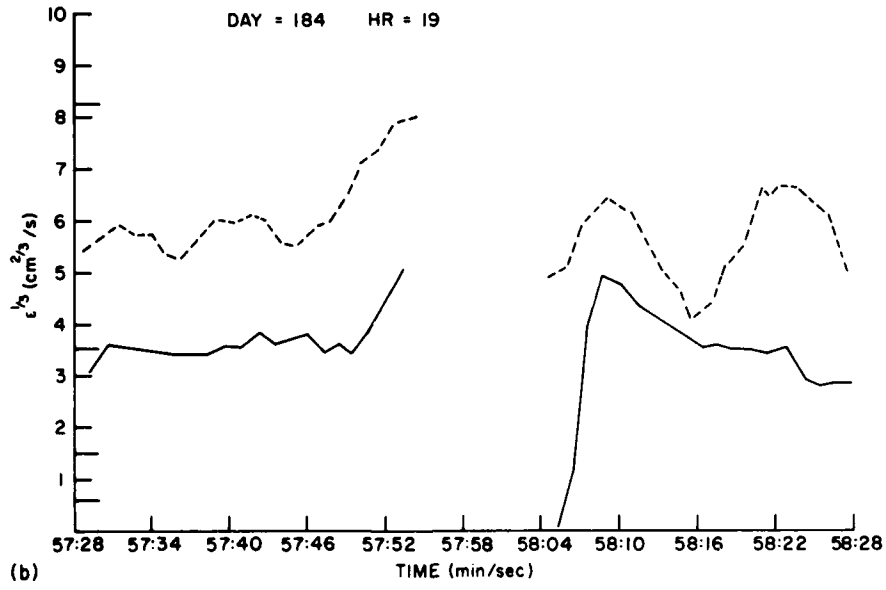

Figure 16. Time History Plots of Turbulence Severity for First Run on 3 July 1981

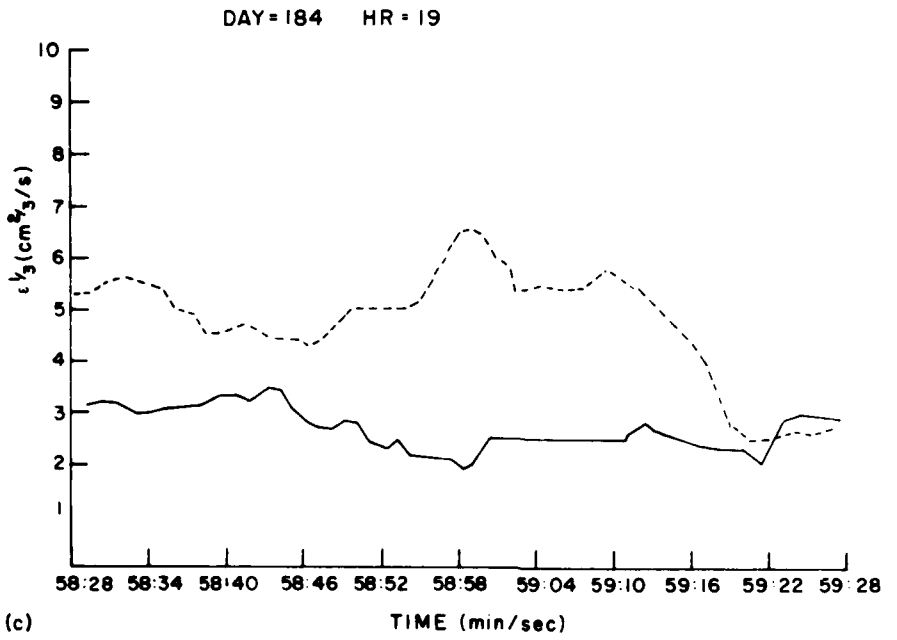

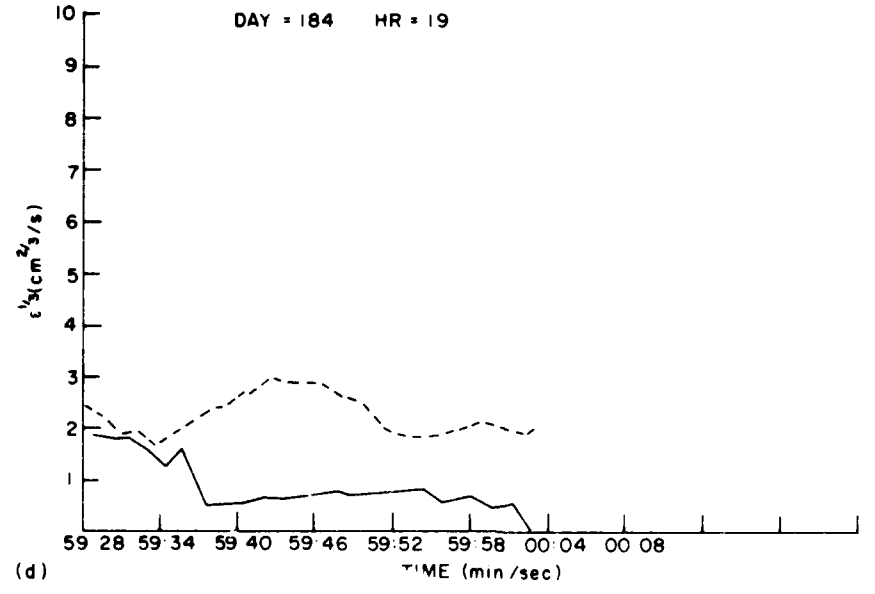

Figure 16. Time History Plots of Turbulence Severity for First Run on 3 July 1981 (Contd)

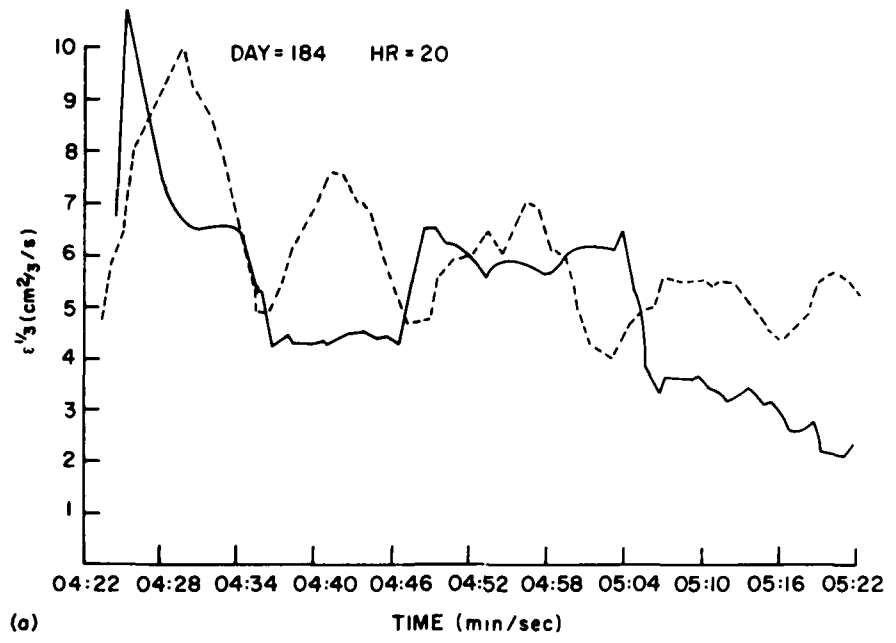

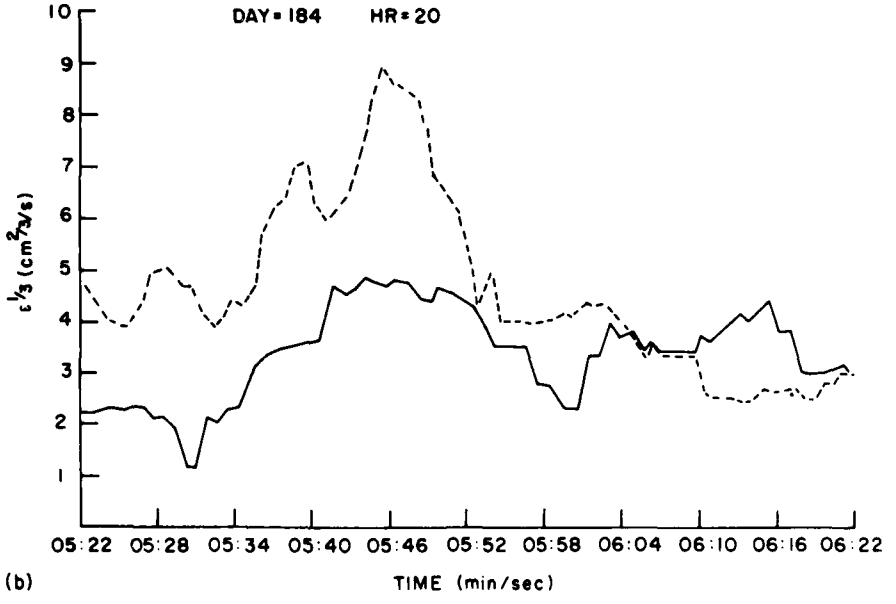

Figure 17. Time History Plots of Turbulence Severity for Second Run on 3 July 1981

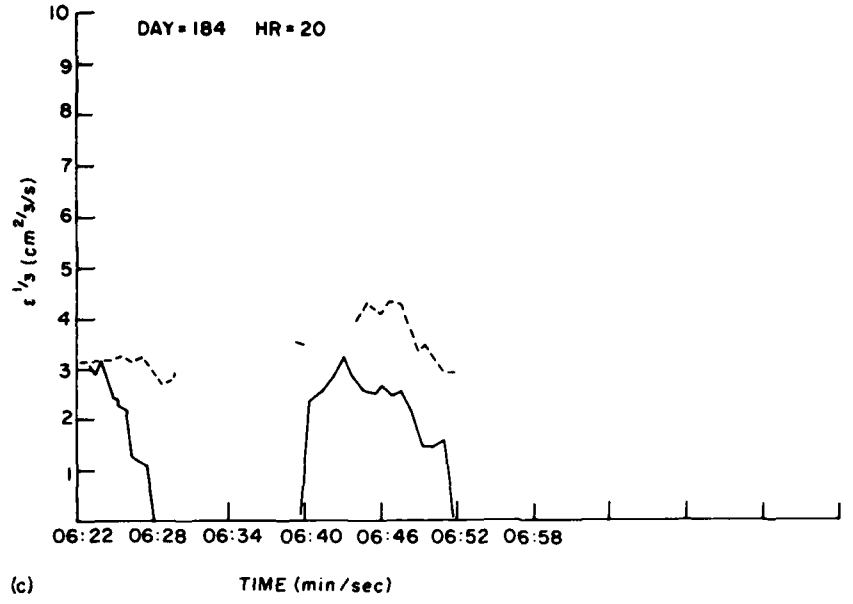

Figure 17. Time History Plots of Turbulence Severity for Second Run on 3 July 1981 (Contd)

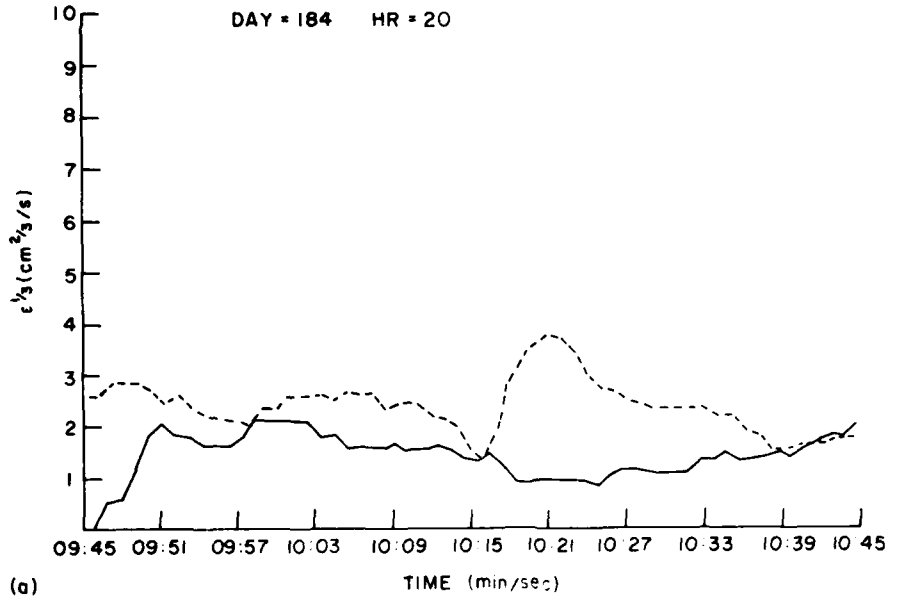

Figure 18. Time History Plots of Turbulence Severity for Third Run on 3 July 1981

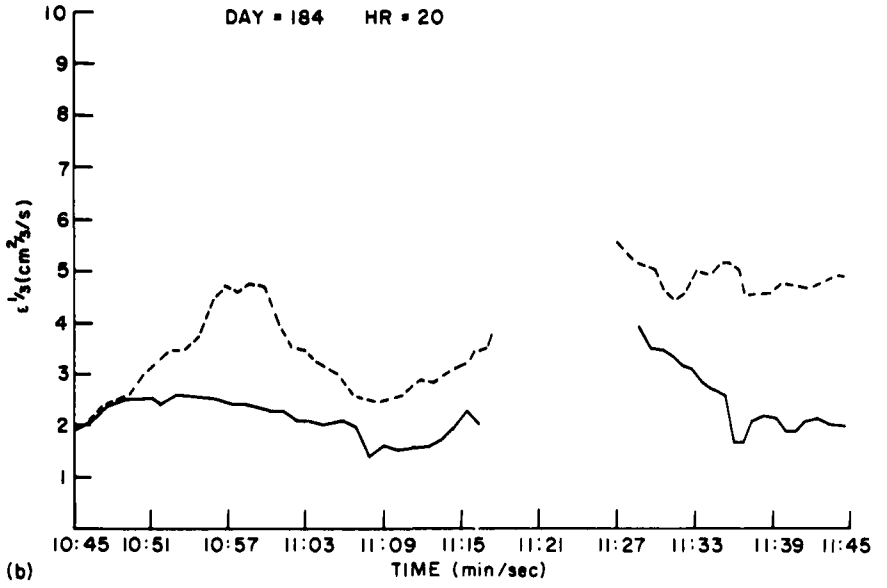

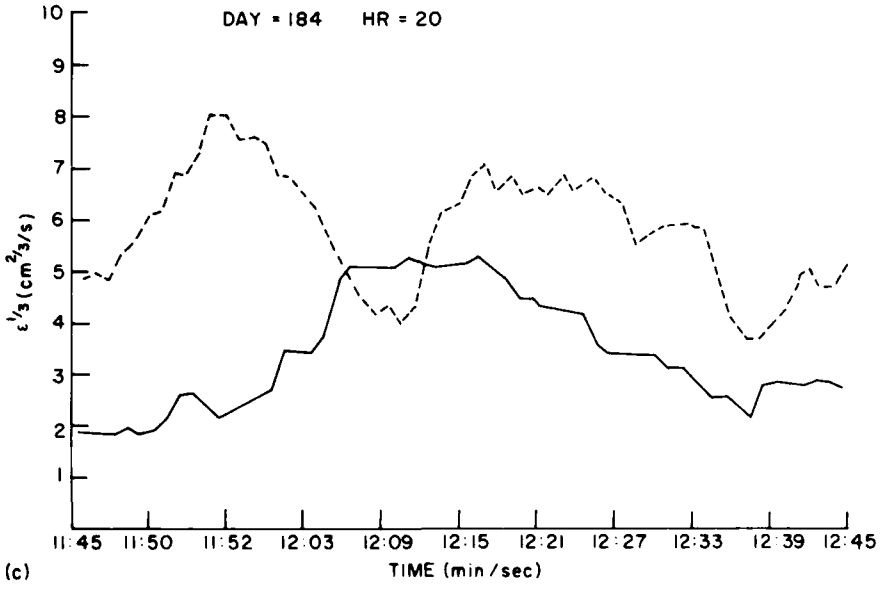

Figure 18. Time History Plots of Turbulence Severity for Third Run on 3 July 1981 (Contd)

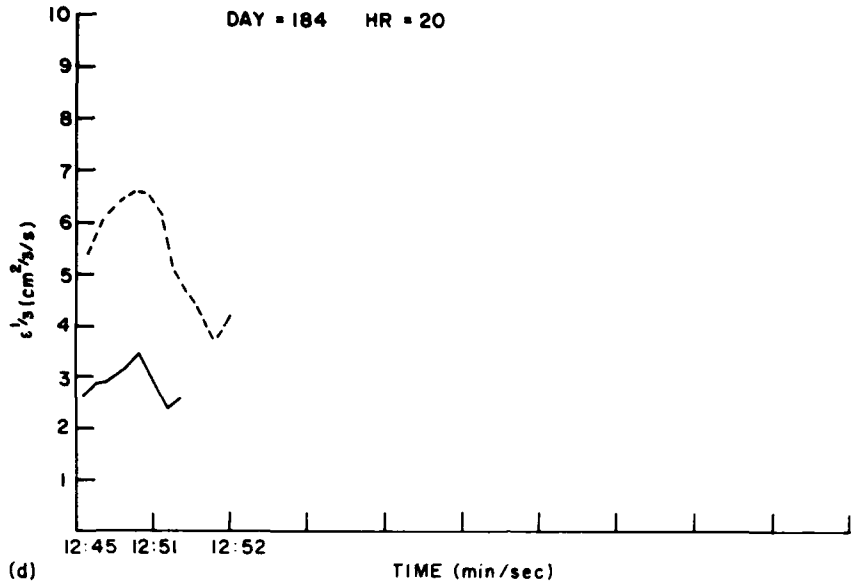

Figure 18. Time History Plots of Turbulence Severity for Third Run on 3 July 1981 (Contd)

Passing through the eastern cell boundary, turbulence severity decreases markedly with the outer scale length being less than 1.8 km. The period near 19:59:30 GMT could, once again, represent a situation where $\lambda_o \ll 1.8$ km and where the STF estimate is strongly biased by radial shear.

During the second penetration (Figure 17), maximum turbulence severity is found at the eastern edge of the near cell and center of the farther cell. However, the period near 20:05:10 GMT, corresponding to the inter-cell region, is also highly turbulent. The patterns of the two estimates are quite dissimilar throughout the near cell, while in-phase through the more distant cell. Beyond the farther cell, the two estimates are roughly equal in magnitude but differ in pattern. These observations suggest that regions of strong storm wind shear within the near cell are biasing the turbulence measurements, in particular, the STF estimates (for example, 20:04:20 GMT). Little storm structure shear and strong turbulence are expected in the farther cell. The outer scale lengths are expected to be less than 1.8 km throughout. Upwind of the farther cell shear of the storm wind field may be contributing significantly to the turbulence estimates.

The third penetration (Figure 18), in reasonably close proximity to the first penetration, exhibits behavior consistent with earlier observations. These are moderate turbulence downwind of the farther cell (20:11:00 GMT), strong turbulence at the western edge (20:11:40 GMT), and within (20:11:57 GMT) the near cell.

The strongly turbulent period at 12:21:00 GMT corresponds to the nondescript 25 dBZ region east of the near cell.

The period near 20:12:09 GMT shows a strong drop in the DSV estimate coincident with a strong rise in the STF value. Figure 12 shows a region of moderate shear of the radial velocity at this time. This may be a period where turbulence strength (ϵ) decreases coincidently with a strong increase in storm structure wind shear. Noting that the STF estimates during this time generally include part or all of the radial velocity data between 20:12:00 to 20:12:21 GMT, this may be a case where storm structure is strongly influencing the STF estimates and may be presenting an inaccurate picture of the turbulence field at this location. This is particularly so since the DSV estimate does not respond in kind.

These data show a complex distribution of moderate to heavy turbulence. The turbulence severity is high, not only within the storm cells, but also at the storm cell boundaries, in between the two cells, and in nondescript 25-dBZ regions outside and downstream of the storm cells. The DSV estimates are generally much greater than the STF values, indicating λ_o less than twice the maximum pulse volume dimension of 0.9 km. The DSV estimates provide a clearer picture of the turbulence strength, while the STF estimates appear to be unreliable due to inclusion of storm structure wind shear.

5.3 16 July 1981

On 16 July 1981 (day 197) a broad area of precipitation moved into the observational region from the west. The sounding data is shown in Figure 19. The environmental wind speed varies from near 0 m/s at the surface to 10 m/s near 3.5 km, and remains at about 12 m/s up to 6 km. At the surface the wind direction is roughly 200^{o}, changes to 270^{o} at 2-km height, and remains nearly constant at 280 through 310 above. Figure 20 shows a reflectivity factor plot at the F106B penetration height of 4.27 km for the time 18:32:37 GMT. The two adjusted aircraft tracks are also shown. The area of interest is a high reflectivity factor cell having a maximum value near 40 dBZ on the western edge of the storm complex. It is located at 113 km west and 130 km south of the SPANDAR radar and comprises an area of about 400 km^2. The first recorded aircraft track begins near the center of the storm cell and extends southward to the storm boundary. The second track flirts with the western edge of the storm.

The storm radial velocity structure is shown in Figure 21. The velocity magnitudes are relatively stable near 5 m/s, except for a small region where the oncoming radial wind is greater than 10 m/s, on the southern edge of the cell. With the environmental wind from the northwest the two aircraft tracks and the radar viewing direction are essentially orthogonal to it, thus the small radial velocities observed. A later scan at 19:00:52 GMT, showing similar size, shape,

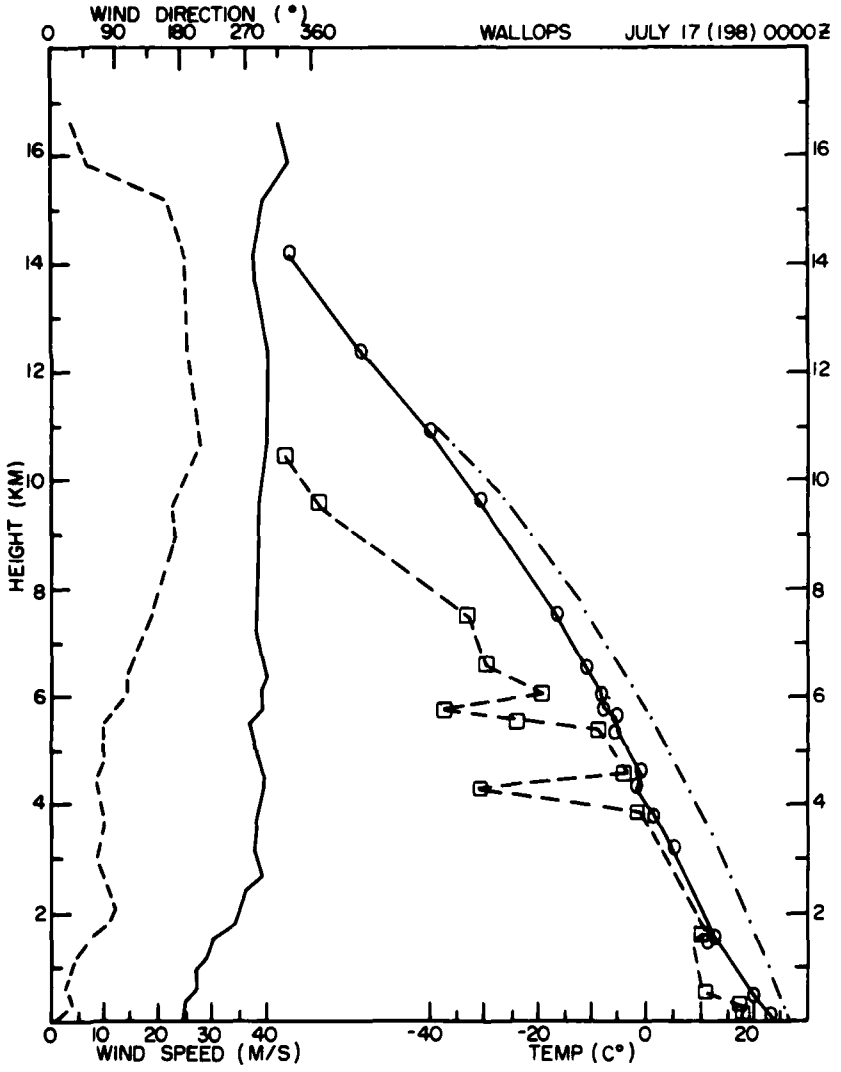

Figure 19. Sounding Data for 17 July 1981 at 00 GMT

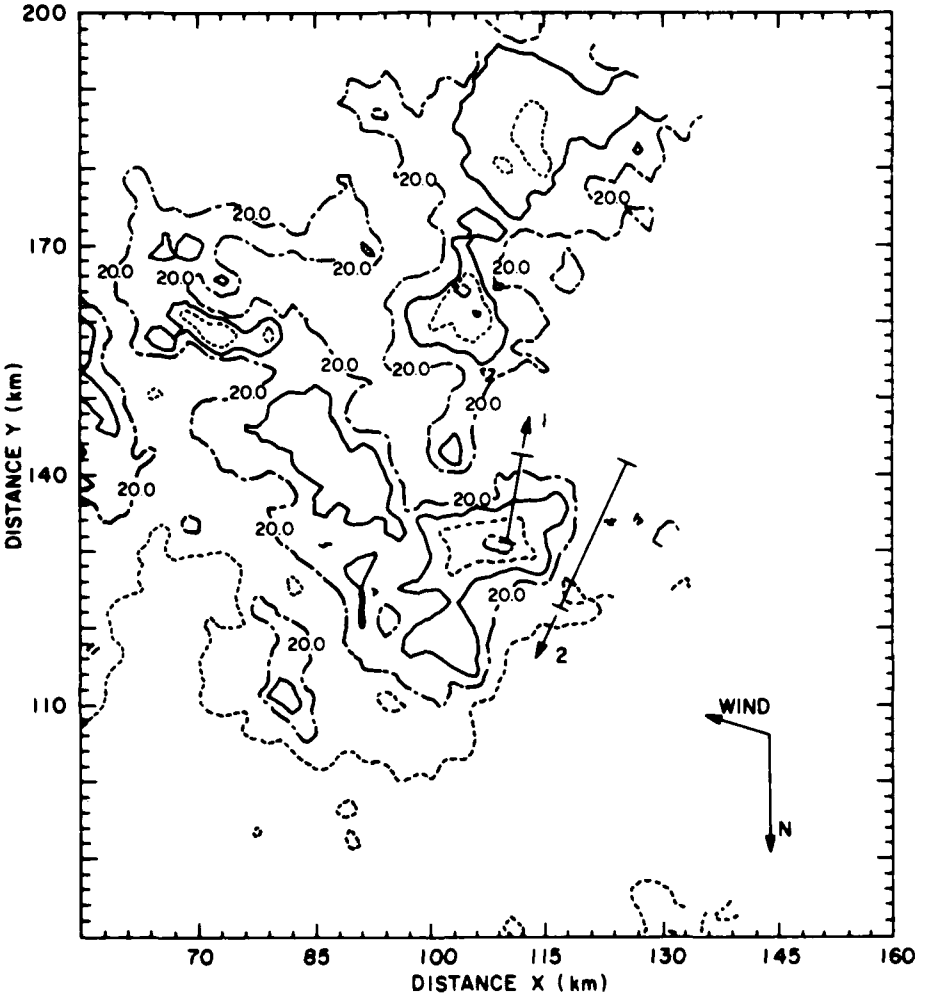

Figure 20. Contours of Storm Reflectivity Factor at Penetration Altitude of 3.5 km for 16 July 1981 at 18:32:37 GMT. Minimum contour value is 15 dBZ

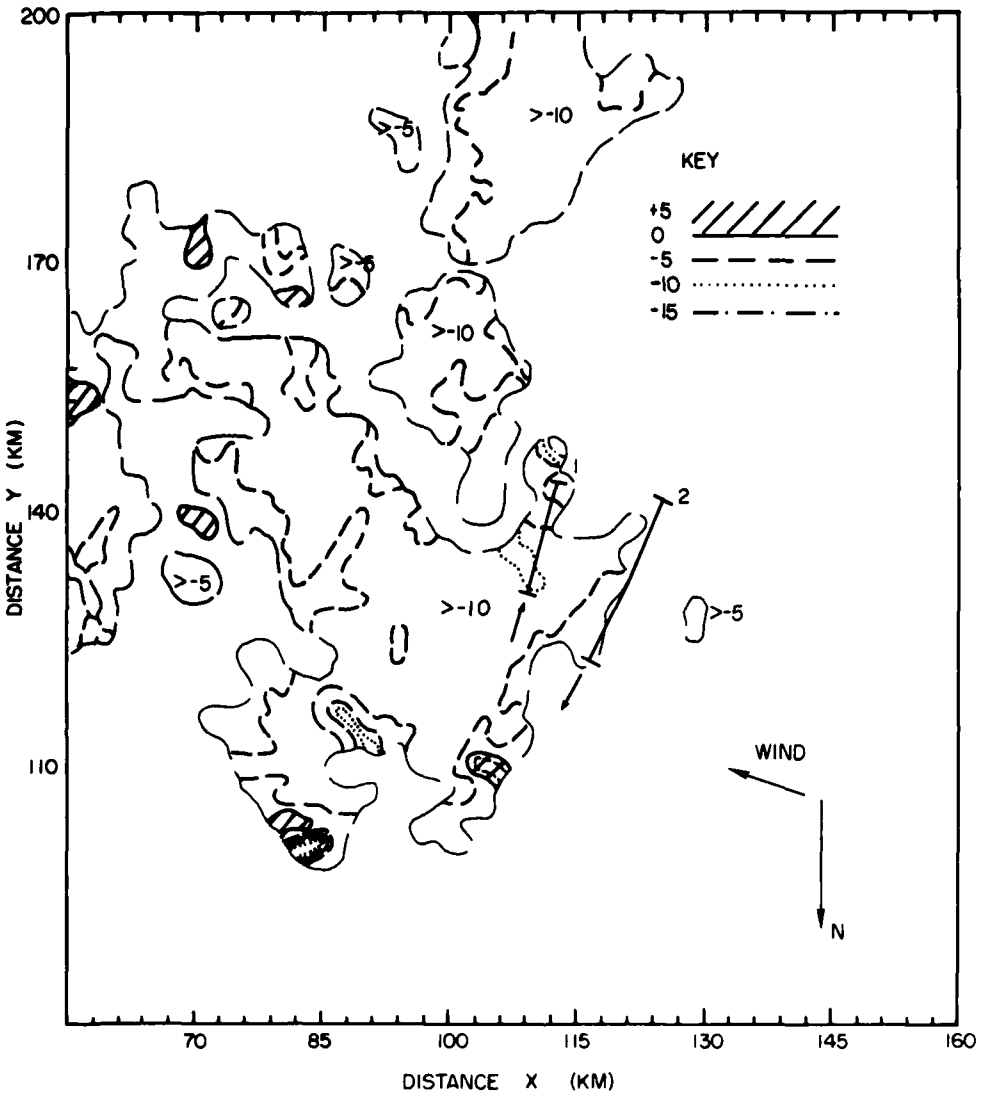

Figure 21. Contours of Storm Radial Velocity at Penetration Altitude of 3.5 km for 16 July 1981 at 18:32:37 GMT

and radial velocity structure, suggests the storm cell region is relatively stationary during the observation period.

The tracking gate spectral velocities are shown in Figures 22 and 23. These histories indicate very little shear of the radial wind along the tracks, with a nearly constant value of -3 to -6 m/s. The tracking gate values agree well with the grid-point values, except for the period near 18:43:55 GMT, where tracking gate data were suspect.

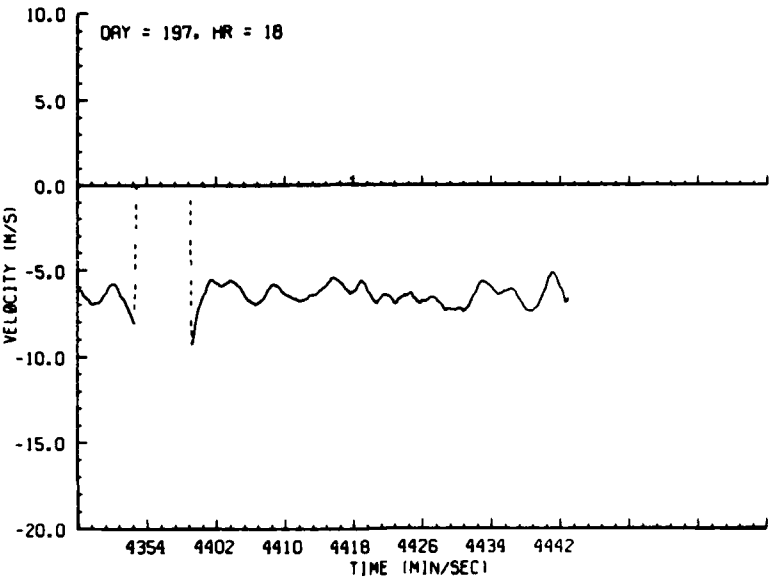

Figure 22. Time History Plot of Tracking Gate Radial Velocity for First Recorded Penetration at 3.5-km Altitude for 16 July 1981

The DSV plots shown in Figures 24 and 25 are also quite uniform, with magnitudes from 0.5 to 3.0 $(m/s)^2$. There is only minor correlation of increased variance with radial velocity gradients, for example at 18:48:23 GMT. Last, there appears to be a slight periodic fluctuation in the velocity and variance plots having a period of 2 to 6 sec. This again suggests perturbations having length scales near 250 to 900 m.

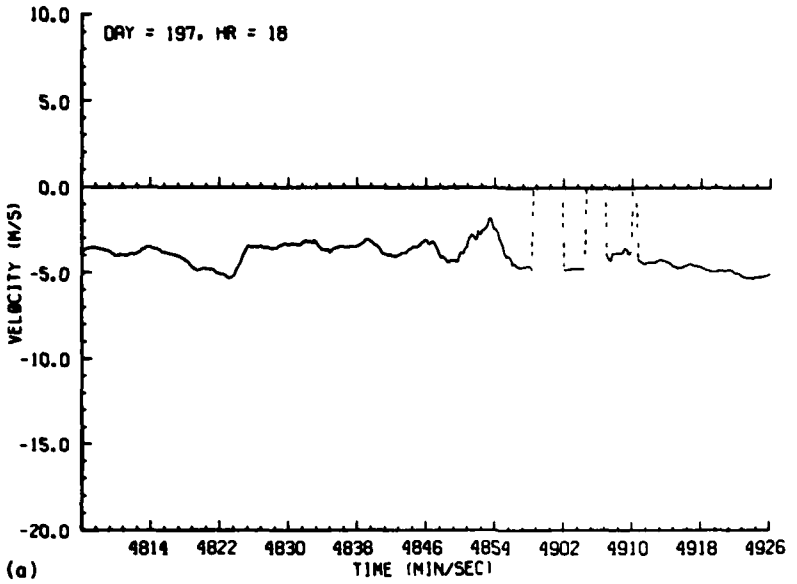

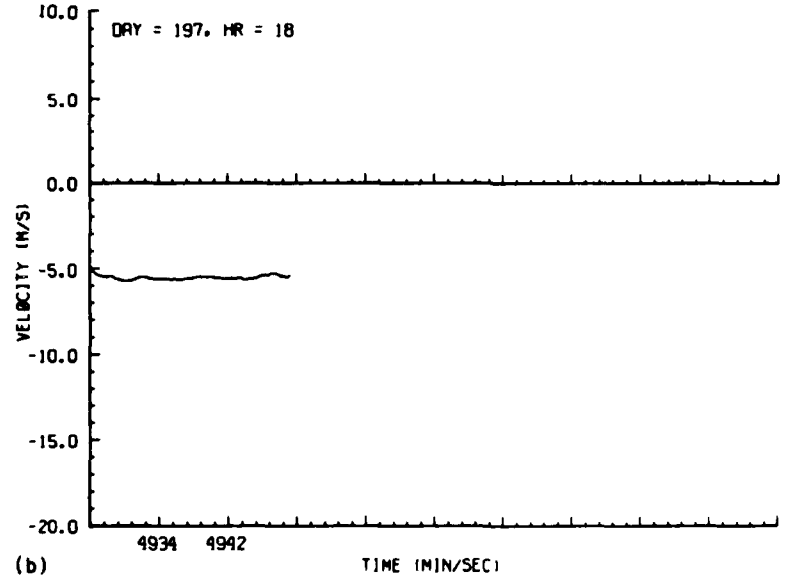

Figure 23. Time History Plot of Tracking Gate Radial Velocity for Second Recorded Penetration at 3.5-km Altitude for 16 July 1981

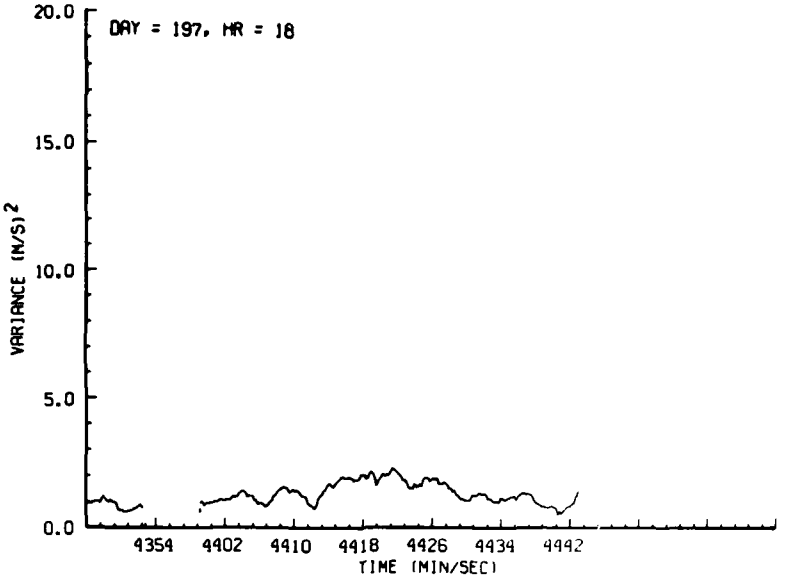

Figure 24. Time History Plot of Tracking Gate Doppler Spectrum Variance (DSV) for First Recorded Penetration at 3.5-km Altitude on 16 July 1981

Figure 26 displays the turbulence severity for the second storm boundary penetration. The block-averaged variance data obtained during the first penetration contained spurious values and were not used in this analysis. The DSV derived estimates exhibit a simple, slowly decreasing, turbulence severity. The STF derived values, on the other hand, show a contradictory increasing magnitude over the first half of the history, while good agreement exists over the latter half. The ever-increasing STF values are believed to result in part from the STF analysis itself. Nonetheless, the features suggest mild turbulence with increasing wind shear during the first half of the penetrations, with mild turbulence and little shear afterwards. The data suggest the outer scale length is probably less than twice the maximum pulse volume dimension of 1.3 km.

5.4 17 July 1981

The final day of observations was 17 July 1981 (day 198). The sounding data are shown in Figure 27. The environmental wind speed increases slowly, from about 2 m/s near 1 km height to about 15 m/s at 5 km height. It then is nearly constant at 14 m/s up to 7 km, where it then gradually increases to 28 m/s at 11 km. The wind direction varies from nearly 130° at the surface to 300° at 2.0 km, and then remains constant above. The storm reflectivity factor is displayed in Figure 28 for the aircraft penetration altitude of 3.35 km. It is a

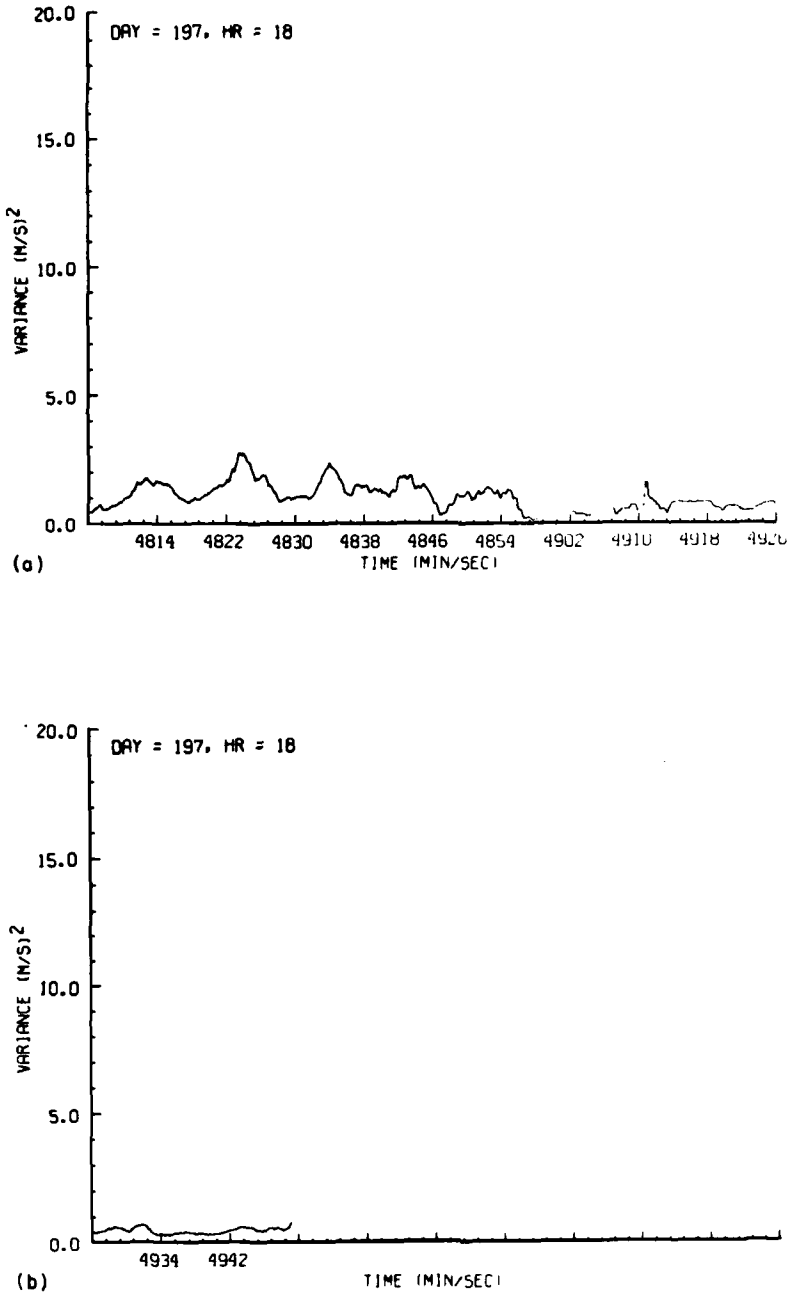

Figure 25. Time History Plot of Tracking Gate Doppler Spectrum Variance (DSV) for Second Recorded Penetration at 3.5-km Altitude on 16 July 1981

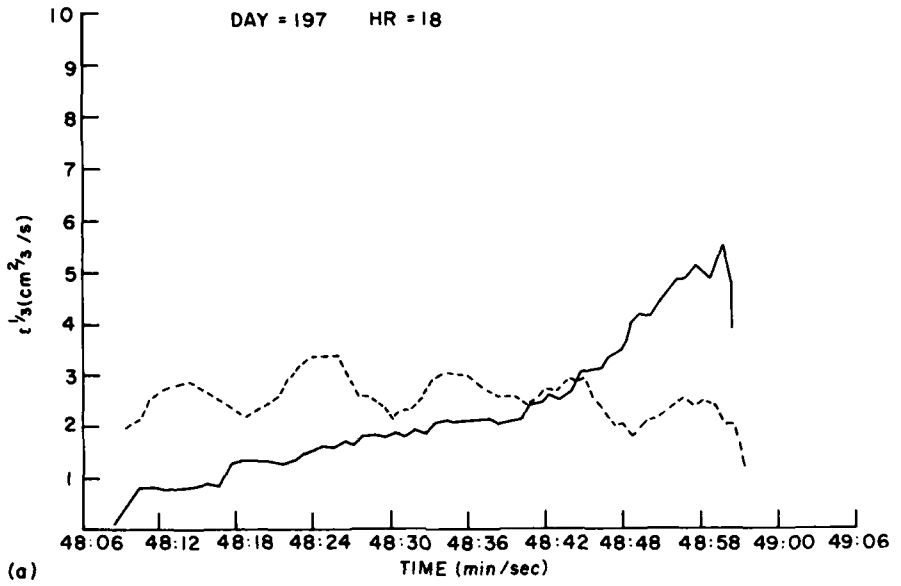

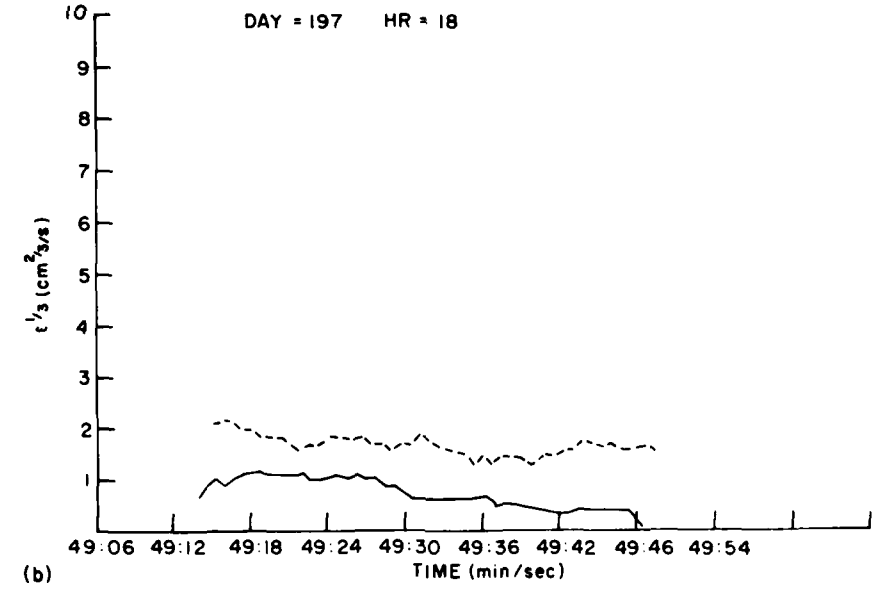

Figure 26. Time History Plots of Turbulence Severity for Second Run on 16 July 1981

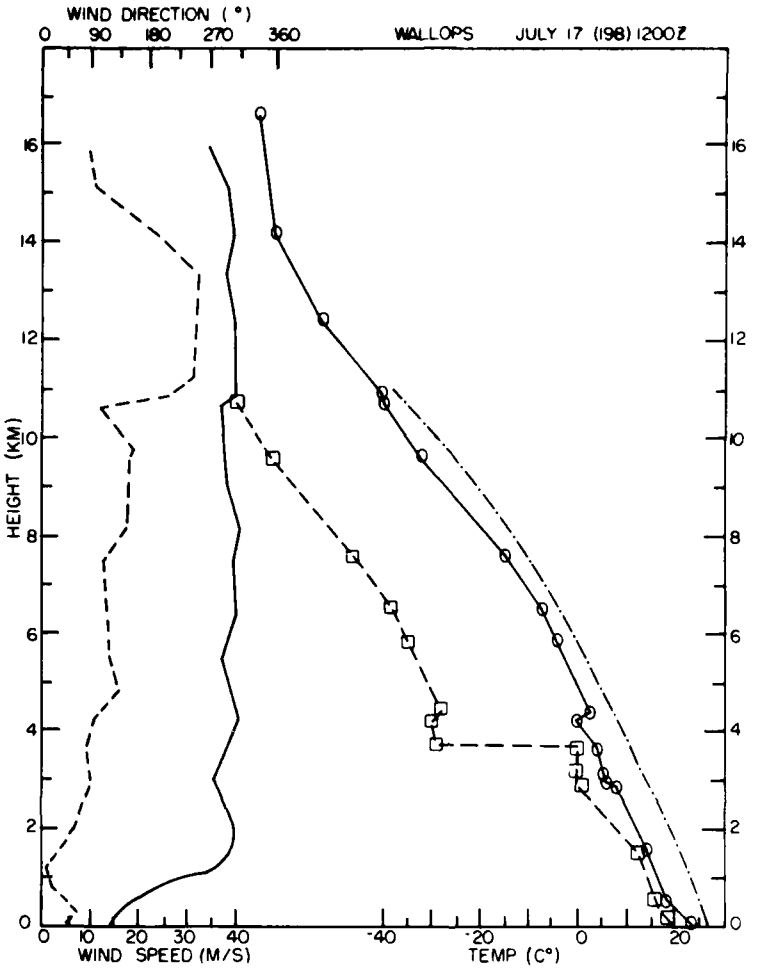

Figure 27. Sounding Data for 17 July 1981 at 1200 GMT

- small complex, with the area of interest located about 80 km due east of the SPANDAR radar. This nearest storm is only about 100 km^2 and is composed of a single high reflectivity factor cell having magnitude near 50 dBZ. The plot time is 18:35:00 GMT. The three adjusted aircraft tracks show the aircraft penetrated the southern and northern boundaries of the storm in regions where the reflectivity factor is 25 dBZ or less.

The corresponding radial velocity plot is shown in Figure 29. This velocity structure is undeniably the most complex of the four days presented. The general trend of increasing magnitude towards the southern boundary reflects the radar scanning more closely along the environmental wind direction. The region of

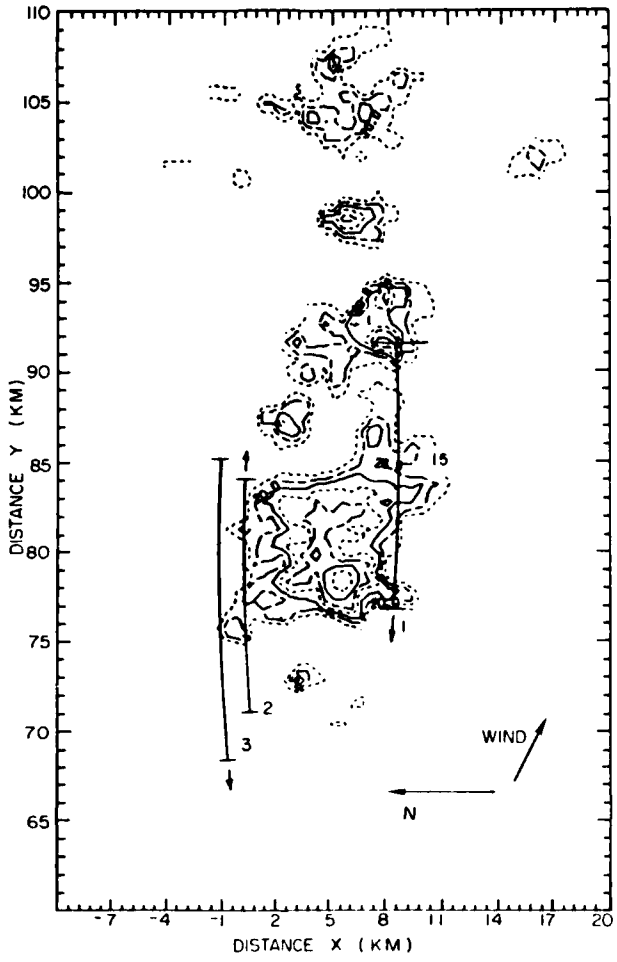

Figure 28. Contours of Storm Reflectivity Factor at Penetration Altitude of 3.35 km for 17 July 1981 at 18:35:00 GMT. Minimum contour value is 15 dBZ

slight increase in radial wind speed, having the appearance of the horseshoe-shaped 5 to 10 m/s region upwind, adjacent to, and downwind of the cell, do however, suggest some divergence of the environmental wind as it encounters the storm. The penetration tracks are roughly 20^{o} off the wind direction.

The time histories of tracking-gate Doppler mean velocity and variance are shown in Figures 30 through 32 and Figures 33 through 35, respectively. The radial velocity histories are in general agreement with the grid-point values. However, the first track shows a reversal in wind direction near 9 km south and 87 km west, between the major storm and the smaller storm further west. It is

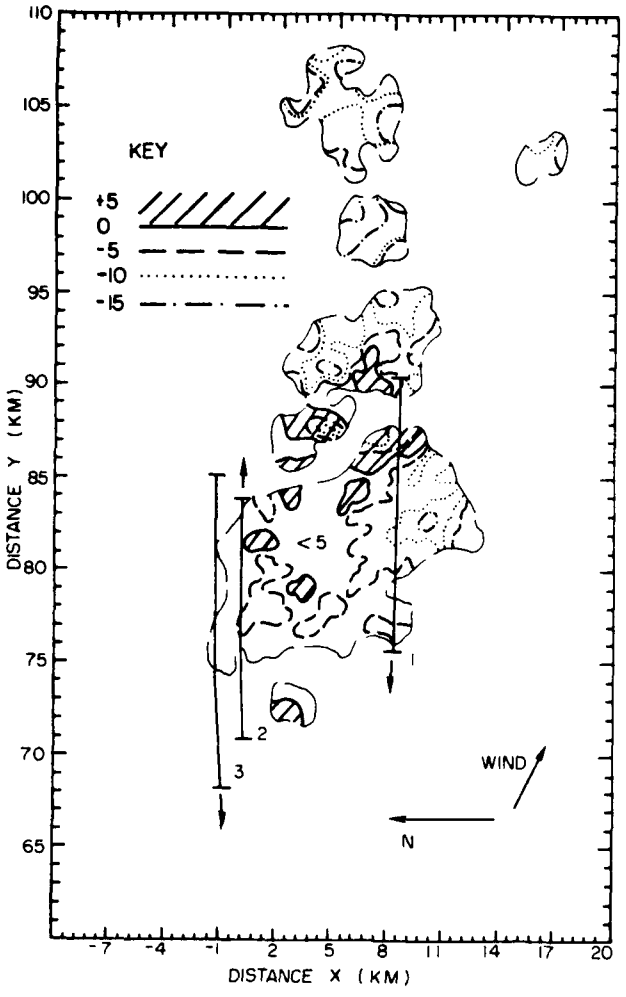

Figure 29. Contours of Storm Radial Velocity at Penetration Altitude of 3.35 km for 17 July 1981 at 18:35:00 GMT.

believed that the pulse-pair velocities here are biased due to low returned power and are considered suspect. The same is true for the region of negative values located 7 km north of this location. In general, the data show a range of velocities from -2 to 9 m/s. The periods of missing data in run 3 indicate the track was skirting the radar detectable northern boundary. Tracks that appear outside the plotted storm boundaries were generally in regions having reflectivity factor of 5 to 15 dBZ.

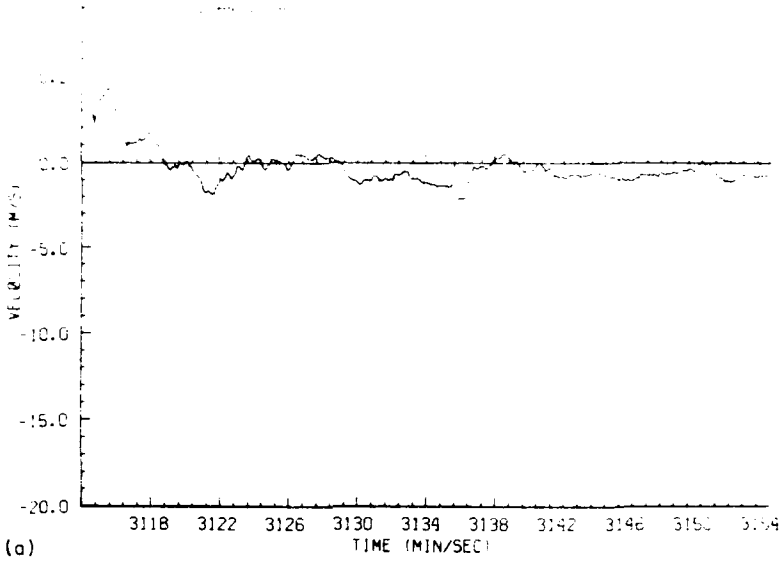

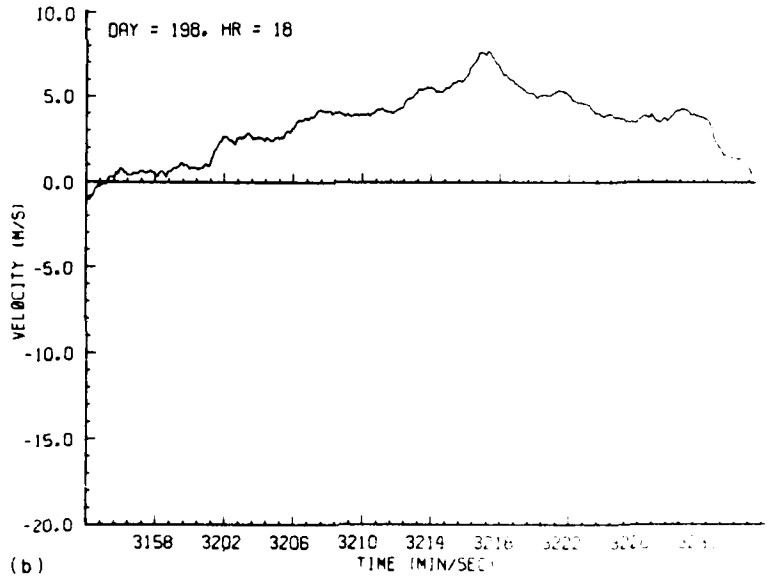

Figure 30. Time History Plot of Tracking Gate Radial Velocity for First Recorded Penetration at 8.85-km Altitude for 17 July 1981

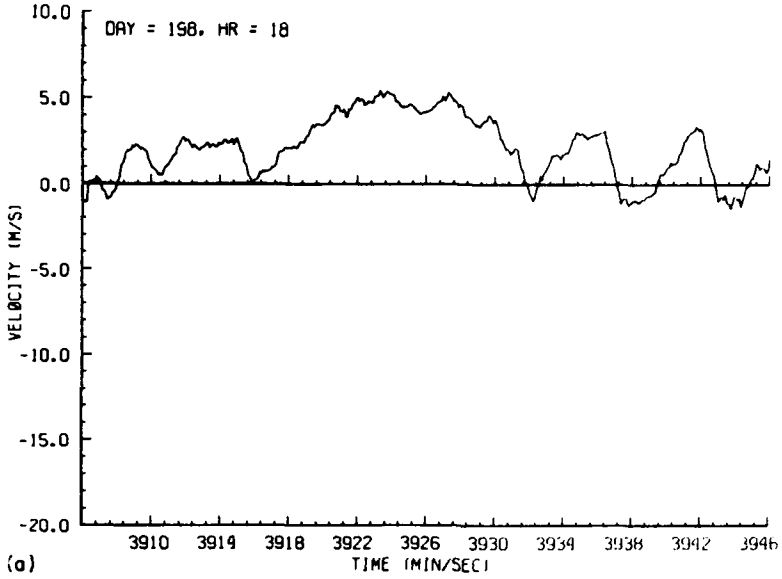

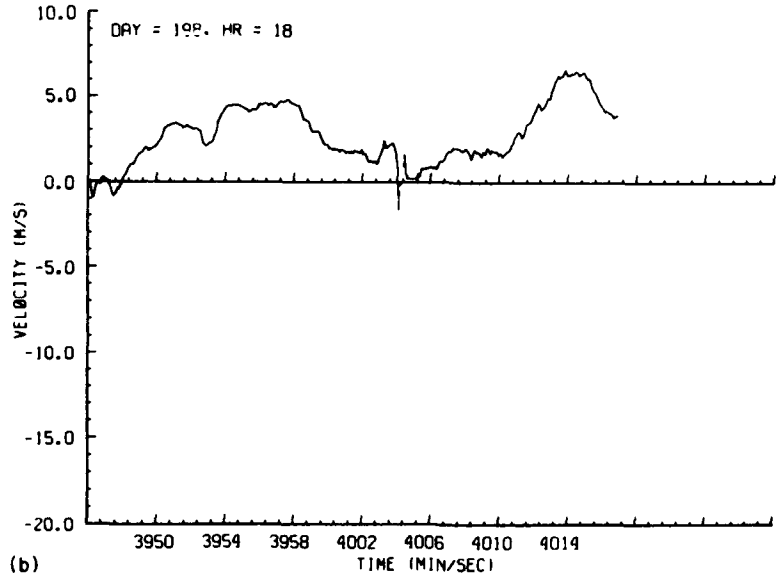

Figure 31. Time History Plot of Tracking Gate Radial Velocity for Second Recorded Penetration at 3.35-km Altitude for 17 July 1981

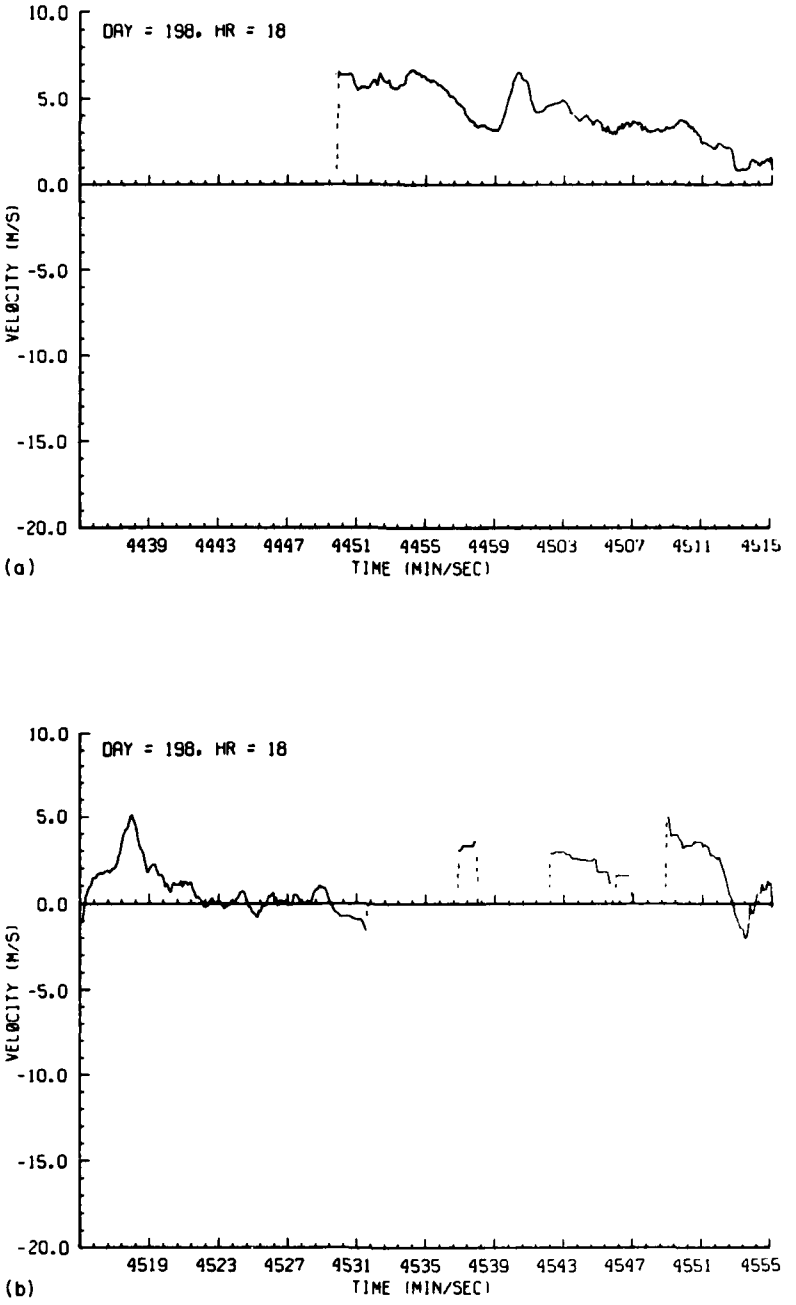

Figure 32. Time History Plot of Tracking Gate Radial Velocity for Third Recorded Penetration at 3.35-km Altitude for 17 July 1981

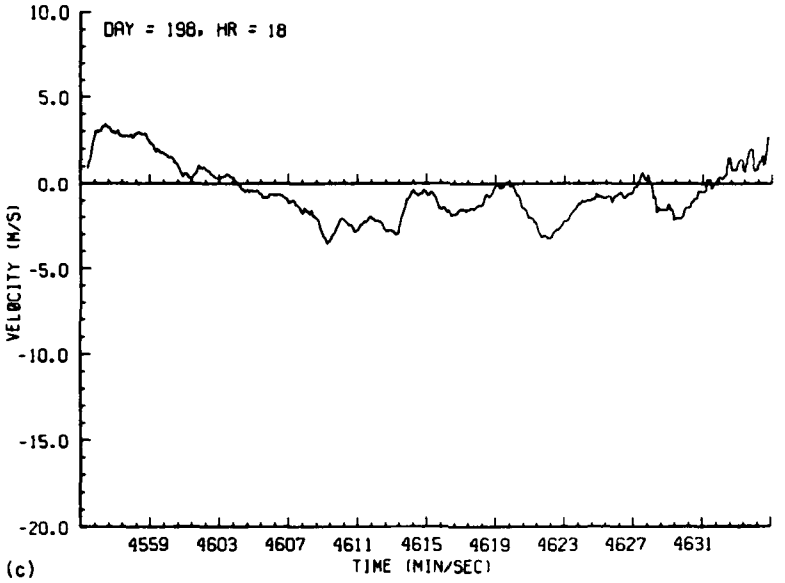

Figure 32. Time History Plot of Tracking Gate Radial Velocity for Third Recorded Penetration at 3.35-km Altitude for 17 July 1981 (Contd)

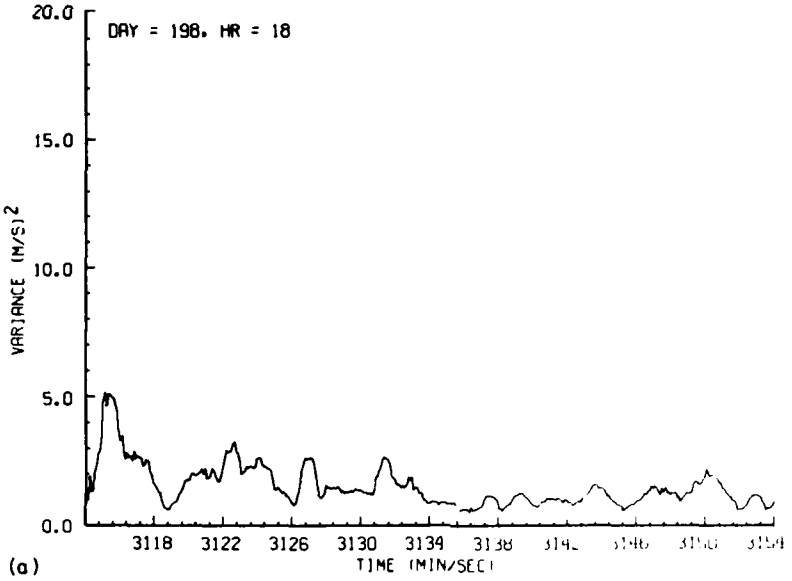

Figure 33. Time History Plot of Tracking Gate Doppler Spectrum Variance (DSV) for First Recorded Penetration at 3.35-km Altitude on 17 July 1981

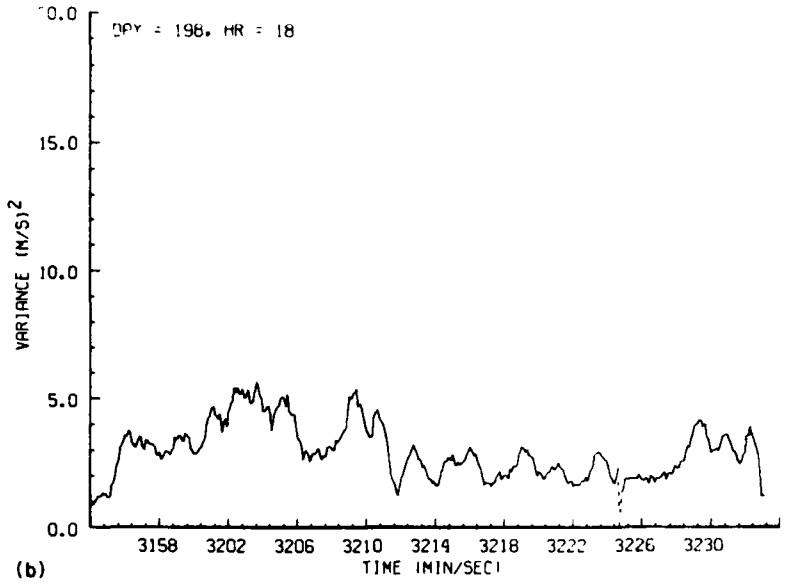

Figure 33. Time History Plot of Tracking Gate Doppler Spectrum Variance (DSV) for First Recorded Penetration at 3.35-km Altitude on 17 July 1981 (Contd)

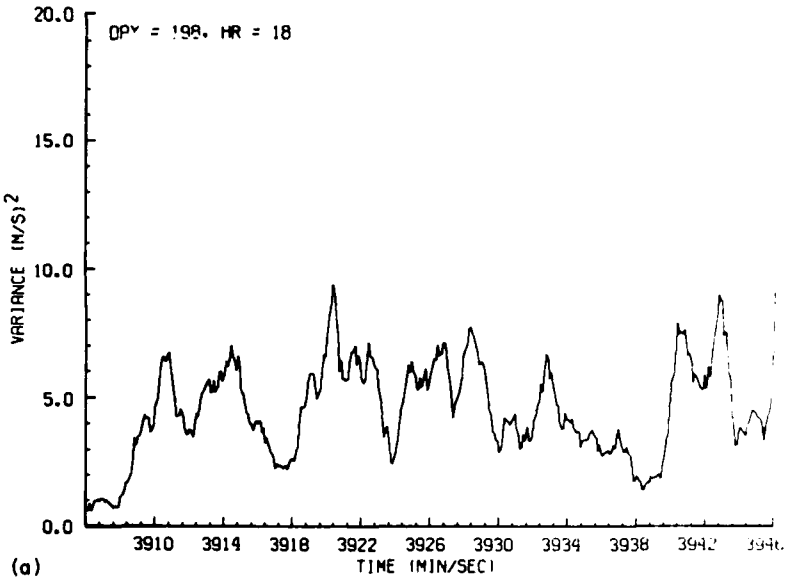

Figure 34. Time History Plot of Tracking Gate Doppler Spectrum Variance (DSV) for Second Recorded Penetration at 3.35-km Altitude on 17 July 1981

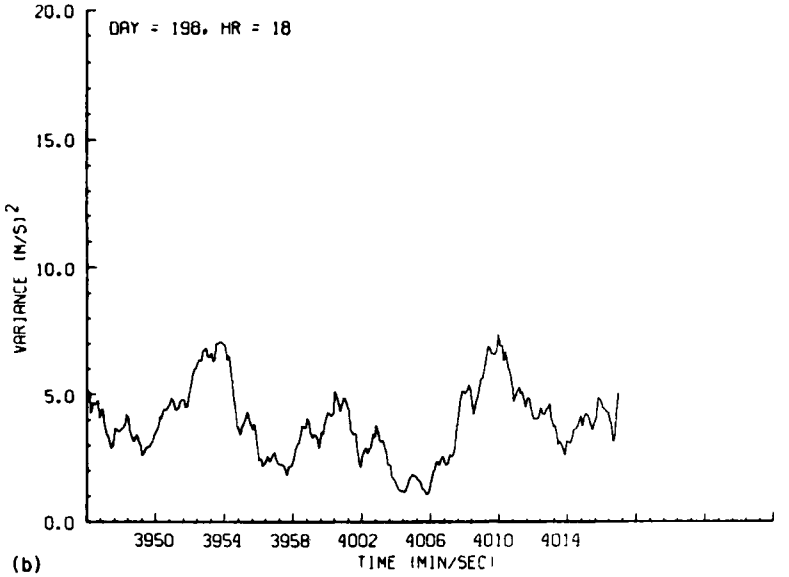

Figure 34. Time History Plot of Tracking Gate Doppler Spectrum Variance (DSV) for Second Recorded Penetration at 3.35-km Altitude on 17 July 1981 (Contd)

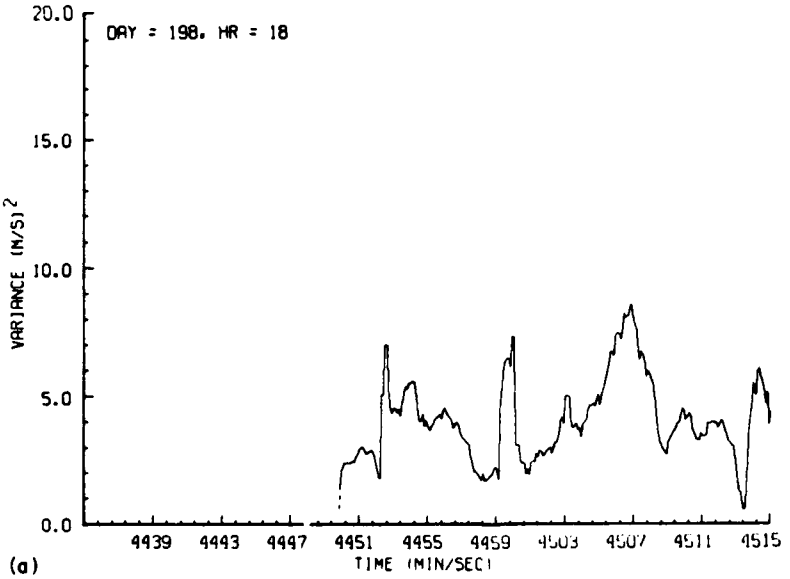

Figure 35. Time History Plot of Tracking Gate Doppler Spectrum Variance for Third Recorded Penetration at 3.35-km Altitude on 17 July 1981

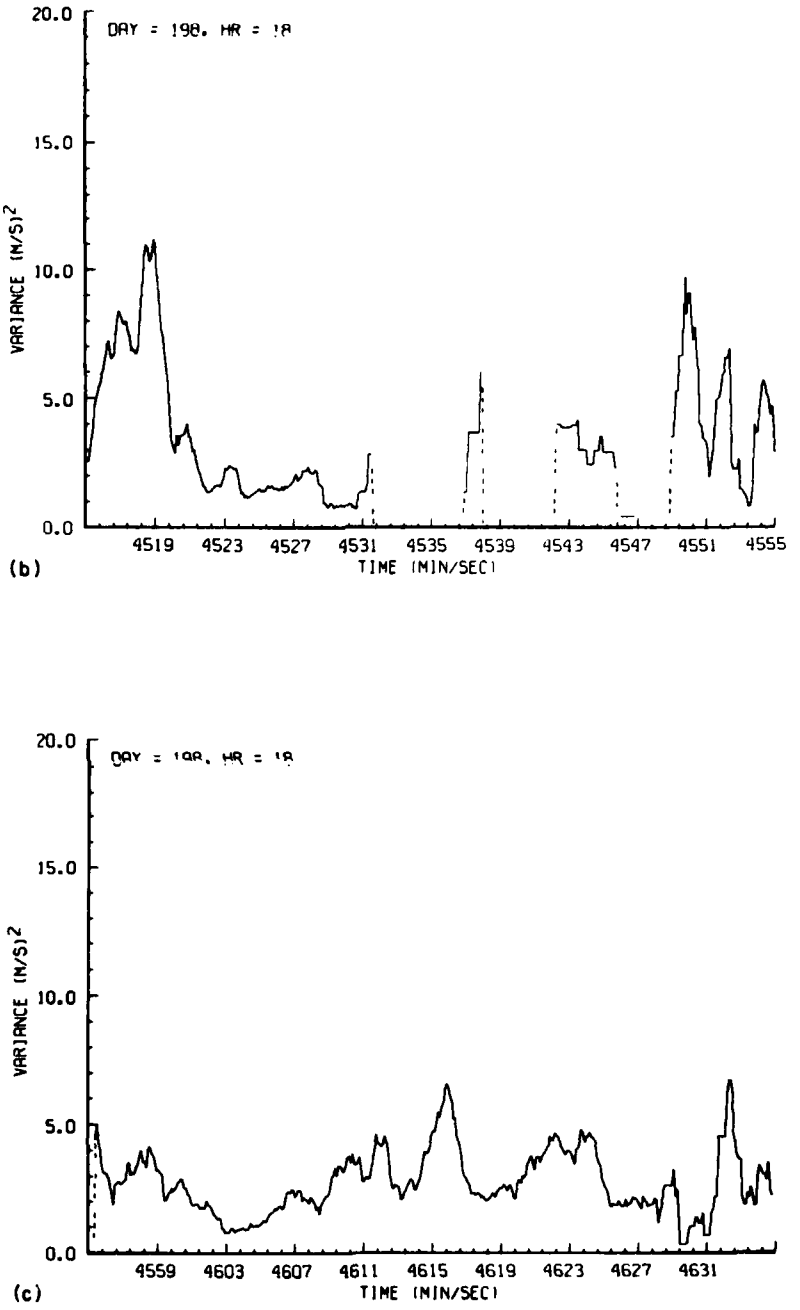

Figure 35. Time History Plot of Tracking Gate Doppler Spectrum Variance for Third Recorded Penetration at 3.35-km Altitude on 17 July 1981

The variance time histories display significant fluctuations, particularly during the latter two penetrations. This is in agreement with the greater fluctuation observed in velocity. One must keep in mind, however, that because of the low signal-to-noise ratio occurring during these two runs, larger scatter about the true Doppler spectrum mean and variance are to be expected. As in previous data, regions of large spectrum variance are only occasionally correlated with strong gradients of the radial velocity. Remaining aware of the potential problems from low signal power, these data suggest, nonetheless, that the large variance values observed result more from strong turbulence than from shear of the large-scale radial wind. Last, observations of the histories suggest that the large variance values observed exhibit fluctuations with preferred periods in the range of 9 to 12 sec, which translate into length scales of about 1.0 to 1.5 km.

Figures 36 through 38 display the turbulence severity estimates for the three recorded penetrations for this day. The pulse volume width is about 0.6 km. The first pass shows reasonably good agreement between the two estimates during the first half of the track. Through the second half the DSV estimates increase dramatically, while the STF estimates remain nearly constant. The STF data suggests that wind shear was not a significant contributor to DSV. However, since the aircraft flew essentially along the radar viewing direction for these flights, no true measure of the transverse storm wind shear is available. These data may also indicate that the significant broadening of the Doppler spectra is due to low signal power, however, one would also expect the STF estimate to increase if this were the case. Thus, the data may suggest a small effective outer scale length, generally increasing in size, but still less than 1.2 km as the plane moves west to east.

The second penetration exhibits similar behavior when the DSV estimate remains relatively constant while the STF values reach a maximum near 18:39:49 GMT. However, the strong radial shear in the radial wind, as is shown by Figure 31, suggests that the STF estimate is biased by storm-structure wind shear.

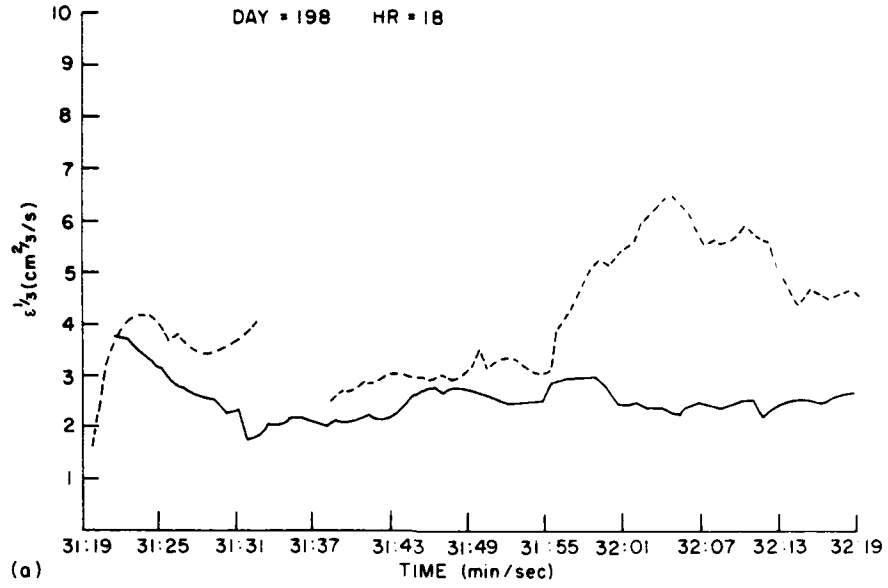

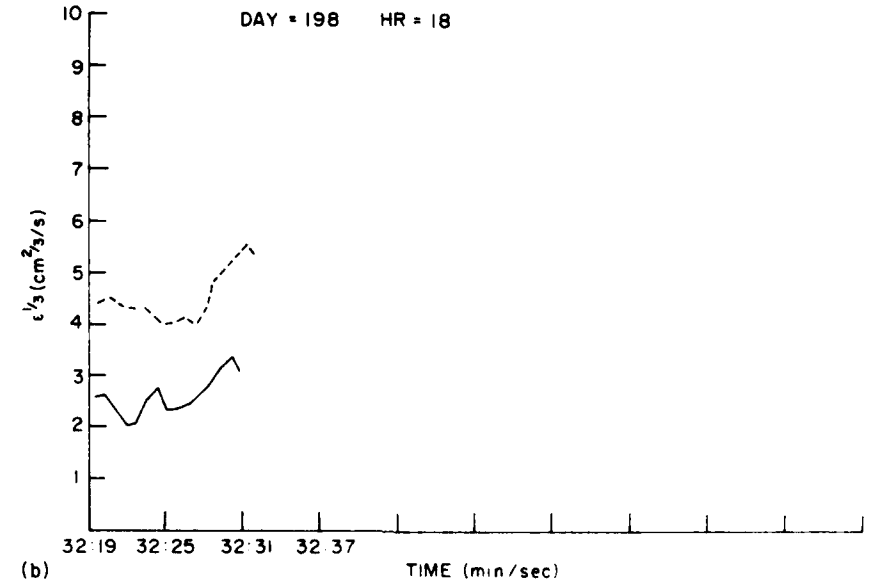

Figure 36. Time History Plots of Turbulence Severity for First Run on 17 July 1981

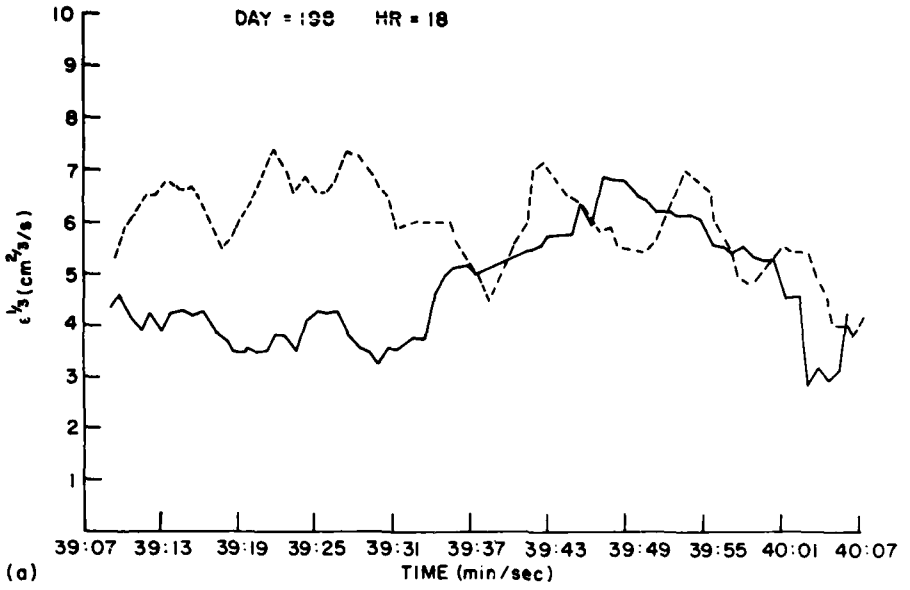

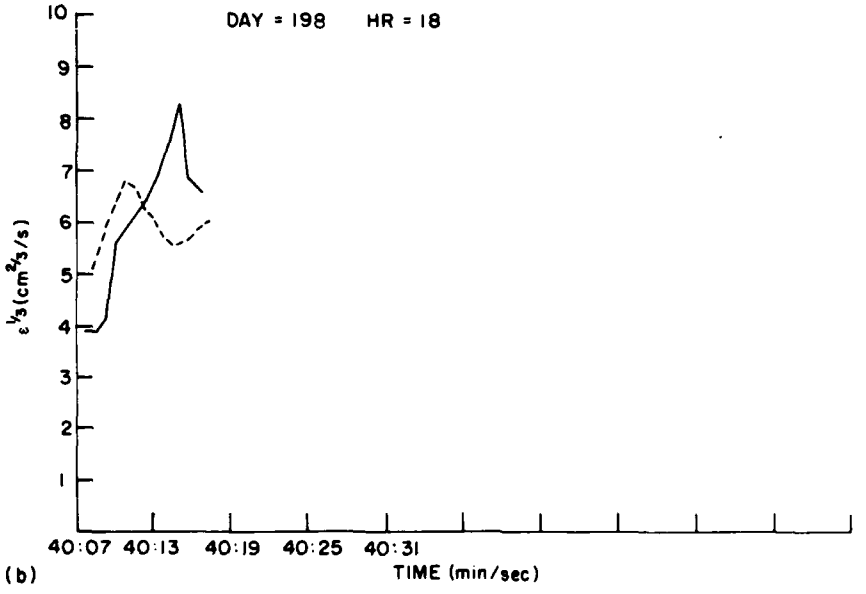

Figure 37. Time History Plots of Turbulence Severity for Second Run on 17 July 1981

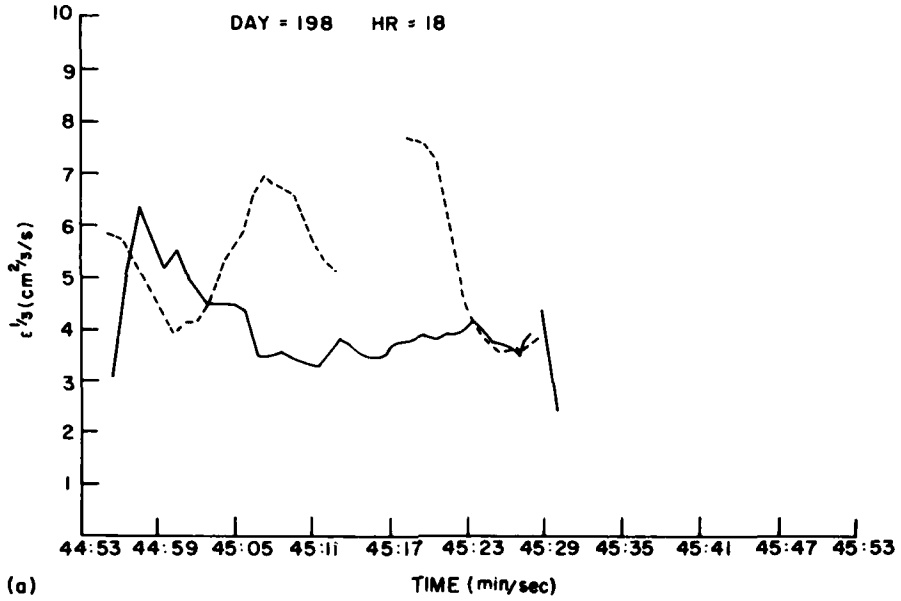

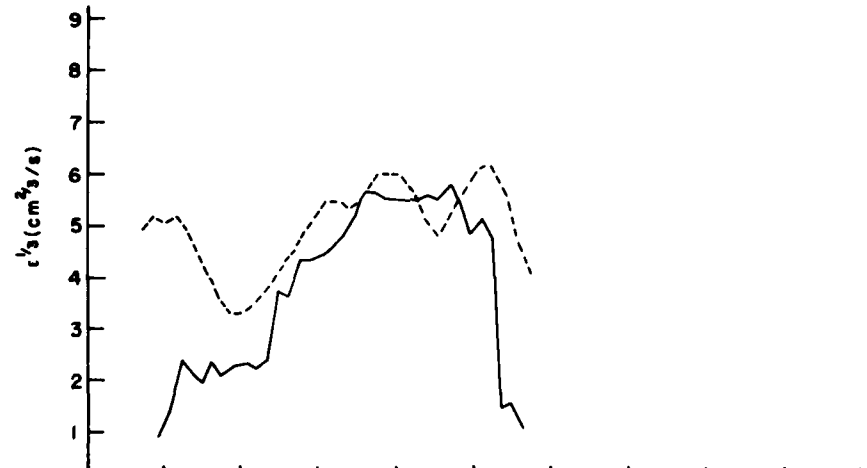

Figure 38. Time History Plots of Turbulence Severity for Third Run on 17 July 1981

6. CONCLUSIONS

The data presented here describe the basic observations made during the 1981 Joint Agency Turbulence field experiment. A total of four aircraft storm-penetration periods were recorded, and resulted in nine spatially and temporally coincident tracking Doppler radar and in-situ aircraft data sets. A variety of environments ranging from nearly uniform, mildly turbulent wind fields, to highly turbulent and complex fields were observed. In most cases the DSV fluctuations observed in the tracking gate data are generally not well correlated with strong gradients of the radial wind field. This suggests that turbulence, rather than wind shear is primarily responsible for the large spectrum variance observed. The time history data also show persistent fluctuations with a range of scales from 200 m to 3.5 km, with the energy content increasing dramatically with increasing scale length. Estimates of turbulence severity show significant turbulence distributed throughout the storm regions. Heavy turbulence is often found not only within high reflectivity factor storm cells, but also in between cells, near storm boundaries, and in innocuous-appearing low reflectivity factor regions. Observations suggest that the turbulence fields are generally characterized by scales of motion less than about 2 km in length. At long range, DSV methods are definitely superior to structure function techniques that do not account for beam filtering effects. Storm-structure wind shear may strongly bias the structure function estimates, but generally do not significantly influence the variance methods. Similar analyses will be performed on the aircraft data, and these data will serve as 'ground truth' for the radar data. These efforts will be used to determine the energy and spatial characteristics of the turbulent fields, and allow for adjustments in the radar methodology. These turbulence analyses will appear in a later report.

END

FILMED

02 — 84

DTIC